Biogeosciences Discuss., 11, 17491–17541, 2014
www.biogeosciences-discuss.net/11/17491/2014/
doi:10.5194/bgd-11-17491-2014

Biogeosciences Discussions
Open Access

Modeling the global emission, transport and deposition of trace elements associated with mineral dust

Y. Zhang[1,2], N. Mahowald[2], R. Scanza[2], E. Journet[3], K. Desboeufs[3], S. Albani[2], J. Kok[4], G. Zhuang[1], Y. Chen[1], D. D. Cohen[5], A. Paytan[6], M. D. Patey[7], E. P. Achterberg[7,9], J P. Engelbrecht[8], and K. W. Fomba[10]

[1]Shanghai Key Laboratory of Atmospheric Particle Pollution and Prevention (LAP3), Department of Environmental Science and Engineering, Fudan University, Shanghai, China
[2]Department of Earth and Atmospheric Science, Cornell University, Ithaca, NYS, USA
[3]LISA, UMR CNRS 7583, Université Paris-Est Créteil et Université Paris-Diderot, Créteil, France
[4]Department of Atmospheric and Oceanic Sciences, University of California, Los Angeles, CA, USA
[5]Australian Nuclear Science and Technology Organization, Locked Bag 2001, Kirrawee DC, NSW, 2232, Australia
[6]Earth and Planetary Sciences Department, University of California, Santa Cruz, CA 95064, USA
[7]Ocean and Earth Science, National Oceanography Centre Southampton, University of Southampton, Southampton SO14 3ZH, UK

[8]Desert Research Institute (DRI), 2215 Raggio Parkway, Reno, Nevada 89512-1095, USA
[9]GEOMAR, Helmholtz Centre for Ocean Research, 24148 Kiel, Germany
[10]Leibniz Institute for Tropospheric Research (TROPOS), 04318 Leipzig, Germany

Received: 13 November 2014 – Accepted: 15 November 2014 – Published: 17 December 2014

Correspondence to: Y. Zhang (yan_zhang@fudan.edu.cn)

Published by Copernicus Publications on behalf of the European Geosciences Union.

BGD
11, 17491–17541, 2014

Abstract

Trace element deposition from desert dust has important impacts on ocean primary productivity. In this study, emission inventories for 8 elements, which are primarily of soil origin, Mg, P, Ca, Mn, Fe, K, Al, and Si were determined based on a global mineral dataset and a soils dataset. Datasets of elemental fractions were used to drive the desert dust model in the Community Earth System Model (CESM) in order to simulate the elemental concentrations of atmospheric dust. Spatial variability of mineral dust elemental fractions was evident on a global scale, particularly for Ca. Simulations of global variations in the Ca / Al ratio, which typically ranged from around 0.1 to 5.0 in soil sources, were consistent with observations, suggesting this ratio to be a good signature for dust source regions. The simulated variable fractions of chemical elements are sufficiently different that estimates of deposition should include elemental variations, especially for Ca, Al and Fe. The model results have been evaluated with observational elemental aerosol concentration data from desert regions and dust events in non-dust regions, providing insights into uncertainties in the modeling approach. The ratios between modeled and observed elemental fractions ranged from 0.7 to 1.6 except for 3.4 and 3.5 for Mg and Mn, respectivly. Using the soil data base improved the correspondence of the spatial hetereogeneity in the modeling of several elements (Ca, Al and Fe) compared to observations. Total and soluble dust associated element fluxes into different ocean basins and ice sheets regions have been estimated, based on the model results. Annual inputs of soluble Mg, P, Ca, Mn, Fe and K associated with dust using mineral dataset were 0.28 Tg, 16.89 Gg, 1.32 Tg, 22.84 Gg, 0.068 Tg, and 0.15 Tg to global oceans and ice sheets.

BGD
11, 17491–17541, 2014

1 Introduction

Desert dust aerosols are principally soil particles suspended in the atmosphere by strong winds, and originate primarily from regions with dry, un-vegetated soils. Desert dust particles are thought to contain several important chemical elements, which can impact the earth system by influencing biogeochemical cycles, and in particularly marine primary productivity (Martin et al., 1991; Duce et al., 1991; Herut et al., 1999, 2002, 2005; Okin et al., 2004; Jickells et al., 2005). Iron (Fe) is considered the most important element carried in dust, and low Fe supplies combined with a low solubility are thought to limit phytoplankton growth in so-called High Nutrient Low Chlorophyll (HNLC) regions. The HNLC regions feature residual macronutrient (e.g. nitrogen (N) and phosphorus (P)) concentrations, but productivity remains low because of the low supply of Fe (e.g. Martin et al., 1991; Boyd et al., 1998). Further studies have linked Fe to the nitrogen cycle, because of high Fe requirements of N fixing organisms (e.g. Capone et al., 1997). While there are internal sedimentary sources of Fe in the ocean, dust deposition is an important source of new Fe to remote regions of the ocean (e.g. Fung et al., 2000; Lam and Bishop, 2008; Moore and Braucher, 2008). Desert dust also contains P, which is a limiting nutrient in some ocean and land regions (e.g. Mills et al., 2004; Okin et al., 2004; Swap et al., 1992), especially on longer time scales. In addition, as a dominant constituent of mineral dust, silicon (Si) is an important nutrient for diatoms which are central in ocean productivity (Morel et al., 2003). Other elements released from mineral dust which may be important for ocean biogeochemistry including manganese (Mn) as a biologically essential nutrient and aluminum (Al) as a tracer of atmospheric inputs (e.g. Nozaki, 1997; http://www.geotraces.org/science/science-plan).

Previous studies have emphasized the importance of measuring elemental composition of dust elements (Kreutz and Sholkovitz, 2000; Cohen et al., 2004; Marino et al., 2004; Marteel et al., 2009), and there are a range of studies highlighting observations of elemental distributions and ecosystem impacts (e.g. Baker et al., 2003; Herut et al., 2002; Buck et al., 2006; Paytan et al., 2009; Chen and Siefert, 2004; Measures and

BGD
11, 17491–17541, 2014

Vink, 2000). In-situ observations show evidence of heterogeneities in elemental fractions over arid soil regions (Svensson et al., 2000; Zhang et al., 2003; Shen et al., 2005, 2006; Li et al., 2007). Ratios between elements including Si, Al, Mg, Ca, and in particular Ca/Al ratios have also been used to distinguish dust source regions, for example for the Asian desert (Zhang et al., 1996; Sun et al., 2005; Han et al., 2005; Shen et al., 2007) and African deserts (Bergametti et al., 1989; Formenti et al., 2008).

Xuan (2005) has simulated the emission inventory of trace elements in dust source regions of East Asia. However, there has not yet been a study to model the distribution of dust associated elements on a global scale. Global dust models usually assume a fixed fraction (e.g. normalized to Al) of each element in dust to simulate global dust elemental transport and deposition, and for example Fe is thought to contribute 3.5 % and P 0.075 % to mineral dust (by mass) (e.g. Luo et al., 2008; Mahowald et al., 2008). Besides spatial variations in elemental compositions, particle size distribution forms another important determinant of elemental abundance in deposited dust. Depending on the particle size distribution, trace elements may remain more or less suspended in the atmosphere and deposited by dry or wet deposition at various distances from desert regions (Seinfeld and Pandis, 1998). There have been very few studies investigating particle size distribution and relate this to elemental concentrations in soil and dust by direct measurement (Schütz and Rahn, 1982; Reid et al., 2003; Castillo et al., 2008; Engelbrecht et al., 2009), and fewer modeling studies have included these phenomena. The ability to model the deposition of specific elements associated with dust in global simulations has been hindered by a lack of understanding of the spatial and temporal variability as well as the particle size distribution associated with different dust sources. As noted by Lawrence and Neff (2009), it seems most appropriate to use a globally averaged value of dust composition to estimate the elemental flux from dust, given the lack of direct measurements of the spatial distribution of elements in dust. However, the use of a global mineral map (Claquin et al., 1999; Nickovic et al., 2012; Journet et al., 2014) and chemical compositions of minerals (Journet et al., 2008) allows us to sim-

BGD
11, 17491–17541, 2014

ulate global elemental inventories from mineral soils, which could be used in a global dust model.

This study aims to introduce a technique to determine a size-fractionated global soil elemental emission inventory based on a global soil and a mineralogical datasets. A companion paper evaluates the ability of the model to simulate mineralogy and the impact on radiation (Scanza et al., 2014). The elemental emission dataset was used as an input to a model simulation of the global dust cycle to present the elemental distributions, which were compared against available observations, and deposition to different ocean regions, estimated for Mg, P, Ca, Fe, Mn, K Al, and Si. Our goal is to assess the variability of elemental fractions in atmospheric and deposited dust, and to investigate whether the elemental emission dataset can adequately predict this variability. This study focuses on desert dust particles, and thus disregards other potentially important sources of the elements such as combustion processes (e.g. Guieu et al., 2005; Luo et al., 2008; Mahowald et al., 2008). We focus on total elemental concentrations, but discuss two methodologies for soluble metal distributions from soil emissions. We also do not consider any atmospheric processing, which is likely to be important for some chemical components (e.g. Mahowald et al., 2005; Baker and Croot, 2010).

2 Materials and methods

2.1 Soil and mineral datasets

The soil map of the world used in this study came from the Food and Agriculture Organization (FAO) of the United Nations soils dataset, and includes 136 soil units (FAO-United Nations Educational, Scientific, and Cultural Organization, FAO-UNESCO, 1976) at a 5 min resolution. The global dataset of soil clay and silt data were used in this study. Following Claquin et al. (1999) and Nickovic et al. (2012), the illite, hematite, kaolinite, smectite, quartz, feldspars, calcite and gypsum contents were specified for different clay and silt soil types, and the global mineral distribution is pre-

BGD
11, 17491–17541, 2014

sented in Scanza et al. (2014). Some minerals found in dust such as dolomite were not considered by Claquin et al. (1999) and Nickovic et al. (2012) and have also been disregarded in this study due to the lack of data on their distribution.

The elemental compositions of hematite and aluminosilicate minerals used in this study are taken from previous works (Journet et al., 2008 and personal communication, Emilie Journet, 2012) and were obtained by *X* ray fluorescence spectrometry (XRF) (Table 1a). Most of minerals used by Journet et al. (2008) are reference materials from the Society's Source Clays Repository, i.e. hematite, illite, kaolinite, montmorillonite. The elemental composition obtained by XRF are in the range of published values for these reference materials (e.g. Mermut and Cano, 2001; Gold et al., 1983), validating the obtained composition for the unreferenced materials. Moreover, the purity of all minerals samples is estimated by X-Ray diffraction. It is noted actual mineralogical maps used in this study do not distinguish feldspars and smectites subtypes. For feldpars, the elemental composition are mostly averaged based on 2 subtype minerals: orthose (potassic feldspar) and oligoclase (sodium-calcium feldspar). For smectites, montmorillonite is the most usually identified smectite in the desert dust (at particularly for Sahara dust e.g. Goudie and Middleton, 2006). The chemical composition of montmorillonite is so used in this study as an analogous of smectite. Forcalcite, gypsum, and quartz, the natural minerals could contain typically substitutions or impurities as clays, which are very variable depending on origin of minerals, formation, contamination etc. The theoretical compositions of elements in calcite, gypsum and quartz are used in this study (Table 1a) since we have not samples to check the chemical compositions of impurities in them. The mass fractions of Ca in calcite ($CaCO_3$) and gypsum ($CaSO_4 \cdot 2H_2O$) are taken as 40 and 23.3 %, respectively. A mass fraction of 46.7 % Si, is used for pure quartz (SiO_2).

Following the total element calculating, soluble elemental fractions were estimated based on soluble elemental contents of minerals at pH = 2 reported by Journet et al. (2008) for the hematite and aluminosilicates, and listed in Table 1b. The fractional solubility of Ca in calcite and gypsum used were 7 and 0.56 %, respectively, and

BGD
11, 17491–17541, 2014

that of Si in quartz was 0.0003 % based on individual solubility product (K_{sp}) at pH = 2 (Petrucci et al., 2001). Here the mineral dependent method is defined as M1. To present uncertainties, the other approach (M2) is introduced as reference. It is based on the extractable fraction of in-situ 20 µm sieved soil samples, reported by Sillanpää (1982) (Table S1) to combine with FAO soil dataset to get a global soluble elemental inventory independent of soil minerals. It is noted that there is no detailed size distribution for soil samples in M2. Thus, the fractions of soluble elements in clay and silt soil are assumed to be equal to the one in the bulk soils themselves.

One drawback of our approach is that we disregard the large variability of soils included within each defined "soil type". The range of minerals within each soil type is large (e.g. Claquin et al., 1999), and the range of elemental concentrations in each mineral is also large (Journet et al., 2008). Our models apply averages, which tends to reduce the variability in elemental composition in the mineral dust in the atmosphere.

2.2 Numerical model description

Community Earth System Model version 1.0.3 (CESM1.0.3) is coordinated by the National Center for Atmospheric Research (NCAR), and has been used to simulate elemental dust emission, transport and deposition in this study. The bulk mineral aerosol in the Community Atmosphere Model version 4 (CAM4) was adapted to include eight trace elements within total dust (Scanza et al., 2014). In this model simulation, the physical scheme CAM4 was driven by the meteorological dataset MERRA, and was simulated spatially at $1.9^{\circ} \times 2.5^{\circ}$ resolution and refered to the years 2000–2010. The soil erodibility map used by the dust model has been spatially tuned (Albani et al., 2014). There were four size classes of dust particles used in the dust emission module in the bulk scheme with particle diameters of 0.1–1.0, 1.0–2.5, 2.5–5.0 and 5.0–10.0 µm. The sub-bin size distribution was assumed to follow a log-normal distribution with a mass median diameter of 3.5 µm (Mahowald et al., 2006) and a geometric SD of 2.0 µm (Zender et al., 2003). Combing these log-normal parameters with the brittle fragmentation theory of dust emission (Kok, 2011) yields each bin's partitioning of dust

BGD
11, 17491–17541, 2014

aerosol mass between the soil's clay and silt size fractions (see Table S3 and Scanza et al., 2014). The elements in the dust undergo three dimensional transport individually in each of the different size bins, identically to bulk dust in the original model. Elemental atmospheric mixing ratios, wet and dry deposition are updated at each model time step based on actual elemental fields and the corresponding tendencies.

2.3 Observational data

An element dataset of ground based aerosol measurements at 17 sites (Fig. 1 and Table S3) was used to evaluate the elemental dust simulation (Sun et al., 2004a, b; Wang et al., 2010; Chen et al., 2008; Engelbrecht et al., 2009; Carpenter et al., 2010; Cohen et al., 2011; Guo et al., 2014; Formenti et al., 2008; Desboeufs et al., 2010). The sites are close to major dust-producing regions across the world as shown in Fig. 1, the observation sites include 10 Asian sites (Central Asia: Hetian, Tazhong; East Asia: Yulin, Duolun, Shengshi; South Asia: Hanoi, and Marnila; Middle East: Balad, Baghdad, Taji), 5 African sites (West Africa: Cape Verde Atmospheric Observatory (CVAO); East Africa: Eilat; North Africa: Tamanrasset, Banizoumbou, and Douz), and 2 Australian sites (Muswellbrook, Richmond). Generally, these field aerosol samples (Total Suspended Particulates (TSP), PM_{10}, $PM_{2.5}$) have 1–3 day collection periods during the period 2001–2010, and were chemically analyzed for elemental contents. No observational aerosol mass concentrations at the Cape Verde station could be used in this study. At this site, the particle matter (PM) concentrations were estimated by assuming an Al to mass ratio of 0.0804. In order to be certain that only desert dust elements are compared with the model results, only data collected during dust storms season were selected. Measurement sites from which data were taken are listed in Table S3, which includes related methodological details.

In addition, the dataset of dust deposition at more than 100 sites worldwide was used to evaluate modeled dust deposition fluxes (Albani et al., 2014).

BGD
11, 17491–17541, 2014

3 Results and discussion

3.1 Fractions of element in arid soil regions

The global distributions of the elements Mg, P, Ca, Mn, Fe, K, Al, and Si in bulk soils as mass percentages in soils are presented in Fig. 2.

3.1.1 Global mapping of soil associated elements

Fractions of elements in soils varied between mineralogical clay and silt fractions. Spatial variability of soil chemistry demonstrated on a global scale (Fig. 2). A large range of variability for some elements within one given source region is observed (e.g. Ca, Fe, Mn, Al). The most extreme variability is observed for Ca in soil silt, which varied from 0.5 to 34.3 %, and was much higher in West and Central Asia, South Africa and Northern South America than in other parts in the world. This is ascribed to the presence of feldspar and gypsum, both being important source minerals for Ca in these regions. In Central and East Asia, the Ca content increased from east to west, showing a similar spatial trend to that reported by Xuan et al. (2005). A south to north gradient of Ca content was also observed in the Sahara following the carbonate distribution of soils (Kandler et al., 2007; Formenti et al., 2011). In southern North Africa, South Africa and the Western Australia, clay soil and fine dust emissions have higher Al and P concentrations than elsewhere. In Eastern Australia, Patagonia, and the northern South Africa, the Fe content of soils is also higher than in other regions. Due to their high content of quartz, soils generally have 25–40 % Si. These elemental distributions are in agreement with other published data for Fe, as they are derived from similar regions (e.g. Claquin, 1999; Hand et al., 2004).

3.1.2 Elemental composition of soils and airborne dust

Trace elements in soils showed different associations with particle size patterns depending on the size distribution of soil minerals, e.g. Mg, P, Fe, Mn, and Al were dom-

BGD
11, 17491–17541, 2014

inant in the clay size fraction (< 2μm) (Fig. 3b). Fractions of Al and Fe reach 11.7 and 3.1 % in clay fractions of soils, while only 2.8 and 1.2 % in silt fractions of soils, respectively. However, Ca and Si showed a slight enrichment in coarser soil fractions. Ca is 2.6 % in clay fractions of soils but 3.6 % in silt soil fractions. This is consistent with the size distribution of Ca and Fe-rich individual particle groupings measured in Sahara dust (Reid et al., 2003). K is almost equally distributed in clay and silt fractions of soils. Taking the fractions of elements in soils as inputs, the fractions of elements in dust emission can be predicted. Our classification of soil particles into four aerosol sizes (Table S2) provides heterogeneity in elements across sizes, but allows for a mixing across soil sizes, reducing the differences among size fractions. For example, the percentage of Fe remained unchanged from clay soil to fine mode dust emission, but changed substantially from silt soil (1.2 %) to coarse mode dust (2.2 % in Bin3). A similar pattern appeared for the other elements, where difference in elemental percentage in the soils is reduced in the dust emissions (Fig. 3a and b).

3.1.3 Elemental dust emissions over desert regions

Annual elemental dust emissions over 15 dust-producing regions (shown in Fig. 1) were determined (Table 2). The annual average of total global dust emission was estimated to be 1582 Tg based on 2001–2010 simulations, and was within the wide range (514 to 5999 $\mathrm{Tg\,yr^{-1}}$) as reported by previous studies (e.g. Shao, 2001; Textor et al., 2006, 2007; Prospero et al., 2010; Huneeus et al., 2011). Africa and Asia accounted for 68 and 31 % of the global emissions, respectively. Correspondingly, trace element emissions were dominant from African desert regions, with percentages ranging between 65–70 %. Specifically, Al emission from Africa accounted for 70 % of global Al emissions, of which 64 % originated from the Western Sahara. For Asian desert regions, elemental dust accounted for 29–34 % of the global total amount, with Ca being the strongest contributor (at 34 %) to global Ca emissions. Iron showed a similar percentage to Al to the total dust emissions with 67 and 32 % of Fe from Africa and Asia, respectively. The maximum contribution for Ca at 5 % was in dust emission from West

BGD
11, 17491–17541, 2014

Asia, being more than 4 times higher than Southern North Africa. However, the fraction of Al and Si was largest in dust emission from Southern North Africa, with values of 9.0 and 31 %, respectively. The fractions of Fe and P were 2.8 %, and 0.08 % in Australia, which is higher than that in other source regions. The simulated elemental fractions showed that differentiating between global source areas is possible and meaningful.

3.2 Spatial and seasonal distribution in fractions of elements in atmospheric and deposited dust

3.2.1 Elemental fractions in global atmospheric dust and deposited dust

The modeled fractions of different elements in atmospheric dust vary substantially on a spatial scale (Fig. 4). Fe content is greater than 2 % for most regions, with a global mean of 2.7 % in atmospheric dust. The maximum contributions of Fe, Al, P and Mn fractions are observed in the tropical Pacific region with values greater than 3, 10, 0.08, and 0.02 %, respectively. For Ca, Si and K, a higher fraction was evident in terrestrial environments. There were obvious land-ocean gradients existing in the distributions of elemental fractions, with higher Ca and Si fractions in terrestrial regions and higher P, Fe, and Al fractions in oceanic areas, likely due to their differences in particle size distribution (Fig. 3). There were very similar spatial partterns and magnitudes shown for the elemental fractions in deposited dust comparing with that in atmospheric dust for each element (Fig. 5). Higher fractionsof Ca and Si in deposited dustis observedin regions close to desert dust sources where the two elements occur in the coarser size fractions. Conversely, lower Mg, P, Mn, Fe and Al contents are found dust deposits close to source regions but are higher over oceans in the finer particle size fractions. The importance of relative location of the source compared to the deposition to the elemental ratio adds complexity in applying simple percentages to dust deposition to obtain elemental deposition amounts.

BGD
11, 17491–17541, 2014

3.2.2 Seasonal variability of elemental fraction

As described above, the fractions of elements in dust fluctuate temporally and spatially on a global scale. There are seasonal variations in dust emissions from various desert regions showing different emission patterns (Fig. S2). The peak periods for dust emissions for various desert regions are consistent with those found by Werner et al. (2002) (Fig. S2). Combining the seasonal cycles in atmospheric dust production with the element distributions in desert regions, the elemental fractions showed large monthly variations but small inter-annual variability during 2001–2010 (Fig. S3). Calcium and Al showed clear seasonal cycles, with Ca having the largest monthly variability, with peak concentration in the period July to September. That is ascribed to the higher Ca content of dust originating in West Asia, Central Asia and Southern Africa, regions which provided large global dust emissions in the period June to September. For the other elements, the peak values usually occurred in the period March to May or November to January, corresponding to the periods that global dust emissions reached a maximum.

We modeled the seasonal variability of these elemental fractions. The monthly variability is calculated by:

$$\text{Monthly variablility (\%)} = \frac{\text{SD of twelve monthly fractions}}{\text{Mean of twelve months fractions}} \times 100 \quad (1)$$

Twelve monthly mean fractions were calculated from ten-years of simulation results while the SDs were calculated from these monthly mean data. Finally, the percentages (Eq. 1) of the SD in monthly mean was derived to describe the variability in elemental fractions of atmospheric dust and deposited dust (shown in Figs. 6 and 7).

The monthly mean variation is greatest for Ca, reaching more than 30 % variability in some regions. The temporal variability of elemental percentages in deposited dust tended to be larger than those in atmospheric dust and showed a greater spatial gradient from land to sea. That is similar to the trend of the elemental fractions in atmospheric and deposited dust (Sect. 3.2.1) since the temporal variation was originally induced by the spatially variable elemental fraction. In the South Indian Ocean and the

BGD
11, 17491–17541, 2014

South Atlantic Ocean, the monthly variability was even higher, ascribed to the combined effect of variability in dust emissions, spatial elemental concentration, and dust transport patterns.

3.3 Spatial Ca/Al distribution in soils and dust plumes

Of specific interest is the Ca/Al ratio in soil, atmospheric dust and deposited dust as this ratio may be indicative of specific source regions (Fig. 8). Of all considered ratios, the Ca/Al ratio in soils showed the greatest variability in relation to the relevant desert region (e.g. Formenti et al., 2011). The Ca/Al ratio ranged mainly between 0.1–1 in clay fractions of soils and 0.5–5.0 in silt fractions of soils (Fig. 8a and b). The maximum Ca/Al ratios reached 160 times the global mean Ca/Al ratio of 1.96 in silt fractions of soils (Fig. 8b), much higher than those of other ratios such as Fe, K, and Mn to Al. Asian desert soils had higher Ca/Al ratios, with values greater than 5 in West Asia and Central Asia. The Ca/Al ratio in dust emissions from Central Asia (1.0–1.6) were higher than in East Asia (~ 0.5), which is close to Ca/Al ratios (1.0–1.7) derived from source profiles of Asian dust (Zhang et al., 1997, 2003), also matching the observed Ca/Al ratios (0.7–1.3) in Asia dust events (Sun et al., 2004a, b; Shen et al., 2007). Also, the Ca/Al ratio in dust emissions in North Africa were below 0.5, confirming the application of the Ca/Al ratio of 0.3 (or 3.8 with Al/Ca) as an indicator of North African dust transport to the eastern United States (Perry et al., 1997). There was also the case for ambient $PM_{2.5}$ dust measured on the Canary Islands (Ca/Al = 1.004). However, this ratio could be larger for PM_{10} or TSP (Engelbrecht et al., 2014). Due to the high Ca/Al ratio (4.0–10.0) in a range of desert soils in some regions including South Africa, yielded Ca/Al ratios in dust emissionsof 1.0, being much larger than those from North Africa. The modeled spatial pattern of Ca/Al ratio in dust emission from Asia and northwest Africa is consistent with the currently available dust pattern compiled by Formenti et al. (2011), but showing relatively lower values for the Central Asian desert region.

BGD
11, 17491–17541, 2014

Despite experiencing mixing of airborne dust from various source regions and as a result of dust processing during transport, the Ca/Al ratios still showed spatial variations in global atmospheric dust and deposited dust. Relative to the Ca/Al ratio in source regions (Fig. 8a, b and c), the Ca/Al ratio in atmospheric dust over most of terrestrial Asia ranged between 0.5–0.8, with a maximum reaching 1.8 (Fig. 8d). Due to the spatial variability of Ca/Al ratio in dust emission (Fig. 9a) and despite the preferential settling during transport of silt fraction which presents the highest Ca/Al variability. The variability in Ca/Al ratio in dust deposited into ocean and onto ice sheets regions are also shown in Fig. 9b. Close to West Asia and Western Sahara higher Ca/Al ratios are noted and the North Indian and Mediterranean areas have a Ca/Al ratio above 0.65 in deposited dust. As the combined downwind region of central Asia and East Asia, the North Pacific has a Ca/Al ratio around 0.5. The Ca/Al ratio in dust deposited over the Atlantic ranged between 0.3–0.4 due to the influence of southern North Africa desert region and East Sahara desert both with low ratios of Ca/Al. Since the soil dataset has a high spatial resolution of 5 min (Fig. 8a and b), there is opportunity to improve the grid resolution of $1.9^{\circ} \times 2.5^{\circ}$ in this study to a finer resolution. It is expected that Ca/Al ratio will show a more spatial heterogeneity when a finer-model resolution is used. We conclude that the Ca/Al ratio can be used to identify different source areas and the model can be used to support the observations.

3.4 Model evaluation with observational data

The averaged modeled fractions of elements in atmospheric dust at each site for the periods for which observations are available are comparable with observations for most of the sites (Fig. 10). In generally, the emission inventories based on mineralogy and elemental compositions are consistent with the available data. A large variability in the % of different elements could be observed at 17 sites for most elements, especially for Ca (Fig. 10c1 and c2). The fraction of Fe in the fine mode is closer to the observational data than that the fraction of Fe is in TSP, implying Fe in clay fractions of soils is more accurate than that for silt. There are only a few reported obsevations of Si is in

BGD
11, 17491–17541, 2014

particular difficult to verify. Based on averaged elemental fractions in TSPs at 13 sites, the correlation coefficients (R) between modelled and observed ones ranged widely (Table 3). Calcium and Al had the highest coefficient of 0.75 and 0.72. However, the R for P, Mn and K were negative. For Fe, the correlation coefficient could reach 0.50 from 0.29 if not considering 3 sites in North Africa, in this area the observational Fe fractions in TSP are high whereas the modeled ones keep low (Fig. 10 e1). The modelled elemental fractions in TSP are close to the observed data, most ratios between which range from 0.7 to 1.6 (Table 3). It is noted that either of median of observed (3.10 %) and modeled (2.9 %) was lower than 3.5 %, which was thought to the fraction of Fe in dust (e.g. Luo et al., 2008; Mahowald et al., 2008).

The averaged fractions of Mg and Mn in dust were underestimated by the model at all observational sites. It should be noted that there are some uncertainities when comparing elemental fractions. When the elemental concentration is divided by particle mass concentration to obtain the elemental fraction, the errors are amplified due to error propagation associated with the combination of the error on the particle mass and that of the element concentrations. Even though the available observational data were chosen from source sites or dust event in non-source regions, the contribution from other sources could be important, especially for fine mode particles. The modeled fraction of Mn and Al in fine particle showed a larger inconsistency than that those in TSP when compared with observations. Some of the descrepancies may be because the model only includes particles up to 10 µm in diameter, while the observations include larger particle fractions such as TSPs. In South Asia, the elemental fractions in dust except for Mn, were always much lower than at another sites, perhaps due to anthropogenic contributions to elemental particle matter concentrations. In particular, many metals in insoluble forms in dust particles could be from other sources such as the refractories and steel industries, construction, biomass burning or volcanic emissions (Castillo et al., 2008; Gaudichet et al., 1995; Hinkley et al., 1999; Paris et al., 2010).

The daily elemental fractions across all times and sites where there is data showed that while the mean of the model was similar to the mean of the observations, there

BGD
11, 17491–17541, 2014

were some systematic differences (Fig. 11a and b). The modeled elemental fractios were not as variable as the observations. This could be due to several issues. First there is a greater variability in the soil mineralogy and elemental composition of minerals than those included in the model (we only include the average values).

Secondly, the dust model could introduce systematic errors, or there could be some-unaccounted anthropogenic particulate sources, modifying the dust aerosol. Also inconsistencies in the collection methods and differences in aerosol sampling periods and times, could yield the observed variations in elements as concluded by Lawrence and Neff (2009).

However, the ranges of the modeled fractions of P, Ca, Fe, K and Al were close to the dominant range of the observational fractions (Fig. 11a and b). The fractions of elements in dust measured are reported to be 0.5–2.3 % for Mg, 0.065–0.2 % for P, 1.0–10.2 % for Ca, 0.028–0.124 % for Mn, 1.3–7.8 % for Fe, 1.2–4.6 % for K, 3.7–12.7 % for Al, and 22.4–35.7 % for Si (Wilke et al., 1984; Reheis and Kihl, 1995; Stoorvogel et al., 1997; Zhang et al., 1998; Yadav and Rajamani, 2004; Goudie and Middleton, 2006; Moreno et al., 2006; Jeong, 2008; Lawrence and Neff, 2009; Formenti et al., 2008; Desboeufs et al., 2010). The modeled elemental fraction in dust for P, Ca, Fe, K and Al and Si were similar to observations. However, the modeled fractions of Mg and Mn were lower (3.4 times and 3.5 times respectively in Table 3) than the observed ones for samples used in this study or of the above cited results. Underestimation of Mg and Mn could be due to a deficiency of minerals contaning high concentrations of Mg and Mn in our model, as dolomite ($MgCO_3$) or palygorskyte ($(Mg, Al)_2Si_4O_{10}(OH) \cdot 4(H_2O)$) are often identified in dust particles for Mg (e.g. Diaz-Hernandes et al., 2011; Kalderon et al., 2009). Moreover, it is known that the chemical composition of minerals could be variable according to the regional origin of minerals and possible impurities. For example, the Mg content in calcite ranges from 0 to 2.7 % in the natural environment (Titschack et al., 2011).

For reference we show the comparison of the modeled deposition vs. observed deposition (Fig. 12). The modeled dust deposition flux agreed well with observations. The

BGD
11, 17491–17541, 2014

Corelation coefficient between modeled and observed dust deposition is 0.86. The median of model to observation ratio is 1.15. Overall the model has been tuned to represent dust deposition, concentration and Aerosol Optical Depth (AOD) (Albani et al., 2014), however the model has difficulty matching both deposition and concentration observations, similar to other models (Huneeus et al., 2011), suggesting more work on dust emission, transport and deposition processes is needed.

3.5 Deposition of total and soluble dust elements over the ocean, land and ice sheets

Comparisons between observations and the model simulations presented here suggest some bias in the model results (Fig. 11 and Table 3), subsequently the model deposition values were adjusted to better match observed measurements (Table 3; Fig. 13). This study suggests significant variability in the elemental fractions in dust deposits (Fig. 13, Table 4), and showed that assumption that the fixed composition of dust being deposited over oceans is unlikely to be correct. Consistent with Mahowald et al. (2008), most dust deposition occurred downwind of dust generating regions bordering the North Atlantic, North Pacific and North Indian Ocean. The Greenland ice sheet accounted for the dominant part of to receive elemental deposition into ice sheets regions, receiving an equal summed amount of elements as those deposited in the whole of South Atlantic Ocean. Iron and P are key elements in the marine ecosystem, with 6.3 Tg Fe and 184 Gg P being added annually to all oceans and ice sheets (Table 5).

Also, the amounts of soluble dust element deposition were determined over different regions (see Sect. 2.1) (Fig. 14). No atmospheric processing of natural dust or other sources of particles (e.g. anthropogenic sources) was included in this simulation. To better understand the uncertainties of soluble elements deposition, estimates from two methods were used (Sect. 2.1) in simulating soluble elemental emission, transport and deposition. Fractional solubility of elements could not be estimated due to the lack of total element data from Method 2 (Sillanpää, 1982). Spatial variations in fractional sol-

BGD
11, 17491–17541, 2014

ubility of elements are identified by Method 1 (mineral method) (Fig. 14). Fractional solubility of Ca increases with distance from source regions because its solubility is higher in clay than in silt (Table 1b). Fractional solubility of modeled P in deposition ranged from 5 to 15 %, with Saharan and Australia dust sources having solubilities averaging ~ 10 %, consistent with Baker et al. (2006a, b). Previous observations suggest a fractional solubility for P of 7–100 % (e.g., Graham and Duce, 1982; Chen et al., 1985; Bergametti et al., 1992; Herut et al., 1999, 2002; Ridame and Guieu, 2002). Fractional solubility of Fe was 0.8–1.2 % in regions (Fig. 14) where clay minerals such as illite play an important role (Journet et al., 2008) with a mean value of 1.17 % of fractional Fe solubility (Table 1b). There were obvious North–South gradient in distribution of fractional solubility of Fe and Al, but with opposing magnitude (Fig. 14). The fractional solubility could not be calculated using Method 2 since total elemental fractions in soil was not reported in Sillianpaa (1982). Thus, the proportions of soluble Fe and K in total dust using two methods were compared with each other. It shows similar distribution pattern but values are different as presented in Fig. 15. The mineral method resulted in lower soluble Ca deposition and higher soluble Mg, P, Mn (Fig. 15). Our results suggest significant differences in the spatial distribution of solubility depending on which dataset is used to estimate soil solubility of elements. It should be noted that the solubility measurements by Sillanpää (1982) were performed at different pH values (pH of 7 vs. 2) and media of extraction (acidified ultrapure waters vs. organic ligands solutions). It is known that pH and organic complexation influence highly the fractional solubility, at least for Fe (e.g. Paris et al., 2011). Thus, that would explain the differences in elemental solubility that we computed for the dust. The soluble elemental deposition over ocean basins and ice sheets were determined using two methods and listed in Table 5. Annual inputs of soluble Mg, P, Ca, Mn, Fe and K from mineral dust using method M1 (M2) were 0.28 (0.30) Tg, 16.89 (7.52) Gg, 1.32 (3.35) Tg, 22.84 (6.95) Gg, 0.068 (0.06) Tg, and 0.15 (0.25) Tg to oceans and ice sheets.

BGD
11, 17491–17541, 2014

4 Summary and conclusions

A new technique combining soil and mineralogical datasets was introduced to estimate the global emission inventory of soil associated elements Mg, P, Ca, Mn, Fe, K, Al, and Si. The spatial elemental dust emissions, transport and deposition were simulated using CESM from 2001–2010. Spatial variability of soil element fractions was characterized globally (Fig. 2), and showed that the use of a constant element fraction in dust across the globe is not consistent with existing observational data for Ca and Al (Figs. 10 and 11). There are few observations for elemental distributions in source regions to verify these emission, concentration and deposition simulations, but for some elements (Ca and Al), the soil elemental distribution combined with the transported dust flux in the model better captured the percentage of chemical elements in dust concentrations observed (Figs. 10 and 11). However, both Mg and Mn levels were underestimated by the model using the mineral maps. The correlation of the percent of element at different sites was not statistically significant for several elements (Mg, Mn, P and K), suggesting that improvements in the soil inventories or simulations is required, although these results could also be due to low number of observations. The observations and model results suggest the elemental fractions in dust varied globally and between different dust production regions, especially for Ca with highest values of 30 % and lowest of 1 %. The ratio of Ca/Al, ranged between 0.1–5.0, and is confirmed as an indicator of dust source regions (Zhang et al., 1997, 2003; Sun et al., 2004a, b; Shen et al., 2007). For Fe in TSP, the median of modeled fraction was 2.90 %, less than 3.5 %, a flat value usually used in dust model study (e.g. Luo et al., 2008; Mahowald et al., 2008).

Seasonal variability of emissions and thus concentration and deposition of most elements were simulated in the model. Also, different soluble elemental datasets showed that the fractional solubility of elements varied spatially. Mineral dust elements deposition fluxes into ocean basins were updated using variable fractional elemental inventory and could have potentially important impacts on evaluating their biogeochemical

BGD
11, 17491–17541, 2014

effects. This study shows that soil emission inventories do a fairly good job at predicting dust elemental concentrations during dust events, except for Mg and Mn. The high spatial heterogeneity in elemental distributions was not captured in the model. In future, these dust emission inventories can be combined with anthropogenic elemental inventories to further improve our understanding of elemental deposition to the oceans.

The Supplement related to this article is available online at doi:10.5194/bgd-11-17491-2014-supplement.

Acknowledgements. We would like to thank the US Department of Defense (DOD) for sharing chemical data from their Enhanced Particulate Matter Surveillance Program (EPMSP), and anonymous reviewers for helpful comments. We acknowledge the support of USA NSF grant 0932946 and 1137716 and DOE-SC0006735. Simulations were conducted on the NSF National Center for Atmospheric Research's supercomputers.

References

Albani, S., Mahowald, N. M., Perry, A. T., Scanza, R. A., Zender, C. S., Heavens, N. G., Maggi, V., Kok, J. F., and Otto-Bliesner, B. L.: Improved dust representation in the Community Atmosphere Model, J. Adv. Model. Earth Syst., 6, 541–570, doi:10.1002/2013MS000279, 2014.

Astitha, M., Lelieveld, J., Abdel Kader, M., Pozzer, A., and de Meij, A.: Parameterization of dust emissions in the global atmospheric chemistry-climate model EMAC: impact of nudging and soil properties, Atmos. Chem. Phys., 12, 11057–11083, doi:10.5194/acp-12-11057-2012, 2012.

Baker, A. R., Kelly, S. D., Biswas, K. F., Witt, M., and Jickells, T. D.: Atmospheric deposition of nutrients to the Atlantic Ocean, Geophys. Res. Lett., 30, 2296, doi:10.1029/2003GL018518, 2003.

BGD
11, 17491–17541, 2014

Baker, A. R., French, M., and Linge, K. L.: Trends in aerosol nutrient solubility along a west–east transect of the Saharan dust plume, Geophys. Res. Lett., 33, L07805, doi:10.1029/2005GL024764, 2006a.

Baker, A. R., Jickells, T. D., Witt, M., and Linge, K. L.: Trends in the solubility of iron, aluminum, manganese and phosphorus collected over the Atlantic Ocean, Mar. Chem., 98, 43–58, doi:10.1016/j.marchem.2005.06.004, 2006b.

Baker, A. R. and Croot, P. L.:. Atmospheric and marine controls on aerosol iron solubility in seawater, Mar. Chem., 120, 4–13, 2010.

Bergametti, G., Gomes, L., Coudé-Gaussen, G., Rognon, P. and Le Coustumer, M.: African dust observed over Canary Islands: Source-regions identification and transport pattern for some summer situations, J. Geophys. Res., 12, 14855–14864, doi:10.1029/JD094iD12p14855.1989.

Bergametti, G., Remoudaki, E., Losno, R., Steiner, E., Chatenet, B., and Buat-Menard, P.: Source, transport and deposition of atmospheric phosphorus over the northwestern Mediterranean, J. Atmos. Chem., 14, 501–513, doi:10.1007/BF00115254, 1992.

Boyd, P., Wong, C., Merril, J., Whitney, F., Snow, J., Harrison, P., and Gower, J.: Atmospheric iron supply and enhanced vertical carbon flux in the NE subsartic Pacific: is there a connection?, Global Biogeochem. Cy., 12, 429–441, 1998.

Buck, C., Landing, W. M., Resing, J. A., and Lebon, G.: Aerosol iron and alumninum solubility in the northwest Pacific Ocean: results from the 2002 IOC Cruise, Geochem. Geophy. Geosy., 7, Q04M07, doi:10.1029/2005GC000977, 2006.

Capone, D. G., Zehr, J. P., Paerl, H. W., Bergman, B., and Carpenter, E. J.: Trichodesmium, a globally significant marine cyanobacterium, Science, 276, 1221–1229, 1997.

Carpenter, L. J., Fleming, Z. L., Read, K. A., Lee, J. D., Moller, S. J., Hopkins, J. R., Purvis, R. M., Lewis, A. C., Müller, K., Heinold, B., Herrmann ,H., Fomba, K. W., Pinxteren, D. v., Müller, C., Tegen, I., Wiedensohler, A., Müller, T., N. Niedermeier, Achterberg, E. P., Patey, M. D., Kozlova, E. A., Heimann, M., Heard, D. E., Plane, J. M. C., Mahajan, A., Oetjen, H., Ingham, T., Stone, D., Whalley, L. K., Evans, M. J., Pilling, M. J., Leigh, R. J., Monks, P. S., Karunaharan, A., Vaughan, S., Arnold, S. R., Tschritter, J., Pöhler, D., Frieß, U., Holla, R., Mendes, L. M., Lopez, H., Faria, B., Manning, A. J., and Wallace, D. W. R.: Seasonal characteristics of tropical marine boundary layer air measured at the Cape Verde Atmospheric Observatory, J. Atmos. Chem., 67, 87–140, doi:10.1007/s10874-011-9206-1, 2010.

BGD
11, 17491–17541, 2014

Castillo, S., Moreno, T., Querol, X., Alastuey, A., Cuevas, E., Herrmann, L., Monkaila, M., and Gibbons, W.: Trace element variation in size-fractionated African desert dusts, J. Arid Environ., 72, 1034–1045, 2008.

Chen, L. , Arimoto R., and Duce R. A.: The sources and forms of phosphorus in marine aerosol particles and rain from Northern New Zealand, Atmos. Environ., 19, 779–787, 1985.

Chen, H.-Y., Fang, T.-H., Preston, M., and Lin, S.: Characterization of phosphorus in the aerosol of a coastal atmosphere: using as equential extraction method, Atmos. Environ., 40, 279–289, doi:10.1016/j.atmosenv.2005.09.051, 2006.

Chen, Y. and Siefert, R.: Sesaonal and spatial distributions and dry deposition fluxes of atmospheric total and labile iron over the tropical and subtropical North Atlantic Ocean, J. Geophys. Res., 109, D09305, doi:10.1029/2003JD003958, 2004.

Chen, Y., Paytan, A., Chase, Z., Measures, C., Beck, A. J., Sañudo-Wilhelmy, S. A., and Post, A. F.: Sources and fluxes of atmospheric trace elements to the Gulf of Aqaba, Red Sea, J. Geophys. Res., 113, D05306, doi:10.1029/2007JD009110, 2008.

Claquin, T., Schulz, M., and Balkanski, Y. J.: Modeling the mineralogy of atmospheric dust sources, J. Geophys. Res., 104, 22243–22256, 1999.

Cohen, D. D., Stelcer, E., Hawas, O., and Garton, D.: IBA methods for characterisation of fine particulate atmospheric pollution: a local, regional and global research problem, Nucl. Instrum. Meth. B, 219, 145–152, 2004.

Cohen, D. D., Stelcer, E., Garton, D., and Crawford, J.: Fine particle characterization, source apportionment and long range dust transport into the Sydney Basin: a long term studybetween 1998 and 2009, Atmospheric Pollution Research, 2, 182–189, 2011.

Desboeufs, K., Journet, E., Rajot, J.-L., Chevaillier, S., Triquet, S., Formenti, P., and Zakou, A.: Chemistry of rain events in West Africa: evidence of dust and biogenic influence in convective systems, Atmos. Chem. Phys., 10, 9283–9293, doi:10.5194/acp-10-9283-2010, 2010.

Duce, R. A. and Tindale, N. W.: Atmospheric transport of iron and its deposition in the ocean, Limnol. Oceanogr., 36, 1715–1726, 1991.

Duce, R. A., Liss, P. S., Merrill, J. T., Atlas, E. L., Buat-Me ard, P., Hicks, B. B., Miller, J. M., Prospero, J. M., Arimoto, R., Church, T. M., Ellis, W., Galloway, J. N., Hansen, L., Jickels, T. D., Knap, A. H., Reinhardt, K. H., Schneider, B., Soudine, A., Tokos, J. J., Tsunogai, S., Wollast, R., and Zhou, M.: The atmospheric input of trace species to the world ocean, Global Biogeochem. Cy., 5, 193–259, 1991.

BGD
11, 17491–17541, 2014

Engelbrecht, J., McDonald, E., Gillies, J., Jayanty, R. K. M., Casuccio, G., and Gertler, A. W.: Characterizing mineral dusts and other aerosols from the Middle East – Part 1: Ambient sampling, Inhal. Toxicol., 21, 297–326, 2009.
Engelbrecht, J. P., Menendez, I., and Derbyshire, E.: Sources of $PM_{2.5}$ impacting on Gran Canaria, Spain, Catena, 117, 119–132, doi:10.1016/j.catena.2013.06.017, 2014.
FAO-Unesco: Soil Map of the World, Southeast Asia, 1976, Sheet IX, Edition I, 1976.
Formenti, P., Rajot, J. L., Desboeufs, K., Caquineau, S., Chevaillier, S., Nava, S., Gaudichet, A., Journet, E., Triquet, S., Alfaro, S., Chiari, M., Haywood, J., Coe, H., and Highwood, E.: Regional variability of the composition of mineral dust from western Africa: results from the AMMA SOP0/DABEX and DODO field campaigns, J. Geophys. Res., 113, D00C13, doi:10.1029/2008JD009903, 2008.
Formenti, P., Schütz, L., Balkanski, Y., Desboeufs, K., Ebert, M., Kandler, K., Petzold, A., Scheuvens, D., Weinbruch, S., and Zhang, D.: Recent progress in understanding physical and chemical properties of African and Asian mineral dust, Atmos. Chem. Phys., 11, 8231–8256, doi:10.5194/acp-11-8231-2011, 2011.
Fung, I., Meyn, S. K., Tegen, I., Doney, S., John, J., and Bishop, J.: Iron supply and demand in the upper ocean, Global Biogeochem. Cy., 14, 281–295, 2000.
Gaudichet, A., Echalar, F., Chatenet, B., Quisefit, J. P., Malingre, G., Cachier, H., Buat-menard, P., Artaxo, P., and Maenhaut, W.: Trace elements in tropical African savanna biomass burning aerosols, J. Atmos. Chem., 22, 19–39, 1995.
Gold, C. M., Cavell, P. A., and Smith, D. G. W.: Clay minerals in mixtures: sample preparation, analysis, and statistical interpretation, Clay. Clay Miner., 3, 191–199, 1983.
Goudie, A. S. and Middleton, N. J.: Desert Dust in the Global System, Springer, Berlin, 2006.
Graham, W. F. and Duce, R. A.: The atmospheric transport of phosphorus to the western North Atlantic, Atmos. Environ., 16, 1089–1097, doi:10.1016/0004-6981(82)90198-6, 1982.
Guieu, C., Bonnet, S., Wagener, T., and Loye-Pilot, M.-D.: Biomass burning as a source of dissolved iron to the open ocean?, Geophys. Res. Lett., 22, L19608, doi:10.1029/2005GL022962, 2005.
Guo, L., Chen, Y., Wang, F. J., Meng, X., Xu, Z. F., and Zhuang, G.: Effects of Asian dust on the atmospheric input of trace elements to the East China Sea, Mar. Chem., 163, 19–27, doi:10.1016/j.marchem.2014.04.003, 2014.
Hand, J. L., Mahowald, N. M., Chen, Y., Siefert, R. L., Luo, C., Subramaniam, A., and Fung, I.: Estimates of atmospheric-processed soluble iron from observations and a global

BGD
11, 17491–17541, 2014

mineral aerosol model: biogeochemical implications, J. Geophys. Res., 109, D17205, doi:10.1029/2004JD004574, 2004.
Herut, B., Krom, M., Pan, G., and Mortimer, R.: Atmospheric input of nitrogen and phosphorus to the southeast Mediterranean: sources, fluxes and possible impact, Limnol. Oceanogr., 44, 1683–1692, 1999.
Herut, B., Collier, R., and Krom, M.: The role of dust in supplying nitrogen and phosphorus to the southeast Mediterranean, Limnol. Oceanogr., 47, 870–878, 2002.
Herut, B., Zohary, T., Krom, M. D., Mantoura, R. F. C., Pitta, V., Psarra, S., Rassoulzadegan, F., Tanaka, T., and Thingstad, F. T.: Response of east Mediterranean surface water to Saharan dust: on-board microcosm experiment and field observations, Deep-Sea Res. Pt. II, 52, 3024–3040, doi:10.1016/j.dsr2.2005.09.003, 2005.
Hinkley, T. K., Lamothe, P. J., Wilson, S. A., Finnegan, D. L., and Gerlach, T. M.: Metal emissions from Kilauea, and a suggested revision of the estimated worldwide metal output by quiescent degassing of volcanoes, Earth Planet. Sc. Lett., 170, 315–325, 1999.
Huneeus, N., Schulz, M., Balkanski, Y., Griesfeller, J., Prospero, J., Kinne, S., Bauer, S., Boucher, O., Chin, M., Dentener, F., Diehl, T., Easter, R., Fillmore, D., Ghan, S., Ginoux, P., Grini, A., Horowitz, L., Koch, D., Krol, M. C., Landing, W., Liu, X., Mahowald, N., Miller, R., Morcrette, J.-J., Myhre, G., Penner, J., Perlwitz, J., Stier, P., Takemura, T., and Zender, C. S.: Global dust model intercomparison in AeroCom phase I, Atmos. Chem. Phys., 11, 7781–7816, doi:10.5194/acp-11-7781-2011, 2011.
Jeong, G. Y.: Bulk and single-particle mineralogy of Asian dust and a comparison with its source soils, J. Geophys. Res., 113, D02208, doi:10.1029/2007jd008606, 2008.
Jickells, T., An, Z., Andersen, K., Baker, A., Bergametti, G., Brooks, N., Cao, J., Boyd, P., Duce, R., Hunter, K., Kawahata, H., Kubilay, N., LaRoche, J., Liss, P., Mahowald, N., Prospero, J., Ridgwell, A., Tegen, I., and Torres, R.: Global iron connections between dust, ocean biogeochemistry and climate, Science, 308, 67–71, 2005.
Journet, E., Desboeufs, K. V., Caquineau, S., and Colin, J.-L.: Mineralogy as a critical factor of dust iron solubility, Geophys. Res. Lett., 35, L07805, doi:10.1029/2007gl031589, 2008.
Journet, E., Balkanski, Y., and Harrison, S. P.: A new data set of soil mineralogy for dust-cycle modeling, Atmos. Chem. Phys., 14, 3801–3816, doi:10.5194/acp-14-3801-2014, 2014.
Kandler, K., Benker, N., Bundke, U., Cuevas, E., Ebert, M., Knippertz, P., Rodríguez, S., Schütz, L., and Weinbruch, S.: Chemical composition and complex refractive index of Saha-

BGD
11, 17491–17541, 2014

ran mineral dust at Izaña, Tenerife (Spain) derived by electron microscopy, Atmos. Environ., 41, 8058–8074, 2007.
Kok, J. F.: A scaling theory for the size distribution of emitted dust aerosols suggests climate models underestimate the size of the global dust cycle, P. Natl. Acad. Sci. USA, 108, 1016–1021, 2011.
Kreutz, K. J. and Sholkovitz, E. R.: Major element, rare earth element, and sulfur isotopic composition of a high-elevation firncore: sources and transport of mineral dust in central Asia, Geochem. Geophy. Geosy., 1, 1048–1071, 2000.
Lam, P. and Bishop, J.: The continental margin is a key sources of iron to the North Pacific Ocean, Geophys. Res. Lett., 35, L07608, doi:10.1029/2008GL033294, 2008.
Lawrence, C. R. and Neff, J. C.: The physical and chemical flux of eolian dust across the landscape: a synthesis of observations and an evaluation of spatial patterns, Chem. Geol., 267, 46–63, doi:10.1016/j.chemgeo.2009.02.005, 2009.
Li, G., Chen, J., Chen, Y., Yang, J., Ji, J., and Liu, L.: Dolomite as a tracer for the source regions of Asian dust, J. Geophys. Res., 112, D17201, doi:10.1029/2007jd008676, 2007.
Luo, C., Mahowald, N., Bond, T., Chuang, P. Y., Artaxo, P., Siefert, R., Chen, Y., and Schauer, J.: Combustion irondistribution and deposition, Global Biogeochem. Cy., 22, GB1012, doi:10.1029/2007GB002964, 2008.
Mahowald, N.; Baker, A.; Bergametti, G.; Brooks, N.; Duce, R.; Jickells, T.; Kubilay, N.; Prospero, J.; Tegen, I. Atmospheric global dust cycle and iron inputs to the ocean, Global Biogeochem. Cy., 19, GB4025, doi:10.1029/2004GB002402, 2005.
Mahowald, N., Muhs, D. R., Levis, S., Rasch, P. J., Yoshioka, M., Zender, C. S., and Luo, C.: Change in atmospheric mineral aerosols in response to climate: last glacial period, preindustrial, modern, and doubled carbon dioxide climates, J. Geophys. Res.-Atmos., 111, D10202, doi:10.1029/2005JD006653, 2006.
Mahowald, N., Jickells, T. D., Baker, A. R., Artaxo, P., Benitez-Nelson, C. R., Bergametti, G., Bond, T. C., Chen, Y., Cohen, D. D., Herut, B., Kubilay, N., Losno, R., Luo, C., Maenhaut, W., McGee, K. A., Okin, G. S., Siefert, R. L., and Tsukuda, S.: Global distribution of atmospheric phosphorus sources, concentrations and deposition rates, and anthropogenic impacts, Global Biogeochem. Cy., 22, GB4026, doi:10.1029/2008GB003240, 2008.
Marino, F., Maggi, V., Delmonte, B., Ghermandi, G., and Petit, J. R.: Elemental composition (Si, Fe, Ti) of atmosphericdust over the last 220 kyr from the EPICA ice core (Dome C, Antarctica), Ann. Glaciol., 39, 110–118, doi:10.3189/172756404781813862, 2004.

BGD
11, 17491–17541, 2014

Marteel, A., Gaspari, V., Boutron, C. F., Barbante, C., Gabrielli, P., Cescon, P., Ferrari, C., Dommergue, A., Rosman, K., Hong, S., and Hur, S.: Climate-related variations in crustal trace elements in Dome C (East Antarctica) ice during the past 672 kyr, Climatic Change, 92, 191–211, 2009.

Martin, J. H., Gordon, R. M., and Fitzwater, S. E.: The case for iron, Limnol. Oceanogr., 36, 1793–1802, 1991.

Measures, C. and Vink, S.: On the use of dissolved aluminum in surface waters to estimate dust deposition to the ocean, Global Biogeochem. Cy., 14, 317–327, 2000.

Mermut, A. R. and Cano, A. F.: Baseline studies of the clay minerals society source clays: chemical analyses of major elements, Clay. Clay Miner., 49, 381–386, 2001.

Mills, M. M., Ridame, C., Davey, M., LaRoche, J., and Geider, R.: Iron and phosphorus co-limit nitrogen fixation in the eastern tropical North Atlantic, Nature, 429, 292–294, 2004.

Moore, J. K. and Braucher, O.: Sedimentary and mineral dust sources of dissolved iron to the world ocean, Biogeosciences, 5, 631–656, doi:10.5194/bg-5-631-2008, 2008.

Morel, F. M. M., Milligan, A. J., and Saito, M. A.: Marine bioinorganic chemistry: the role of trace metals in the oceanic cycles of major nutrients, in: Treatise on Geochemistry, Vol. 6., Elsevier, Pergamon, Oxford, 113–143, ISBN 0-08-043751-6, 2003.

Moreno, T., Querol, X., Castillo, S., Alastuey, A., Cuevas, E., Herrmann, L., Mounkaila, M., Elvira, J., and Gibbons, W.: Geochemical variations in aeolian mineral particles from the Sahara-Sahel dust corridor, Chemosphere, 65, 261–270, 2006.

Nickovic, S., Vukovic, A., Vujadinovic, M., Djurdjevic, V., and Pejanovic, G.: Technical Note: High-resolution mineralogical database of dust-productive soils for atmospheric dust modeling, Atmos. Chem. Phys., 12, 845–855, doi:10.5194/acp-12-845-2012, 2012.

Nozaki, Y.: A fresh look at element distribution in the North Pacific, EOS T. Am. Geophys. Un., 78, 221–221, doi:10.1029/97EO00148, 1997.

Okin, G. S., Mahowald, N., Chadwick, O. A., and Artaxo, P.: Impact of desert dust on the biogeochemistry of phosphorus in terrestrial eco-systems, Global Biogeochem. Cy., 18, GB2005, doi:10.1029/2003GB002145, 2004.

Paris, R., Desboeufs, K. V., Formenti, P., Nava, S., and Chou, C.: Chemical characterisation of iron in dust and biomass burning aerosols during AMMA-SOP0/DABEX: implication for iron solubility, Atmos. Chem. Phys., 10, 4273–4282, doi:10.5194/acp-10-4273-2010, 2010.

BGD
11, 17491–17541, 2014

Paytan, A., Mackey, K., Chen, Y., Lima, I., Doney, S., Mahowald, N., Lablosa, R., and Post, A.: Toxicity of atmospheric aerosols on marine phytoplankton, P. Natl. Acad. Sci. USA, 106, 106, 4601–4605, doi:10.1073/pnas.0811486106, 2009.

Perry, K. D., Cahill, T. A., Eldred, R. A., Dutcher, D. D., and Gill, T. E.: Long-range transport of North African dust to the eastern United States, J. Geophys. Res.-Atmos., 102, 11225–11238, 1997.

Petrucci, R. H., Harwood, W. S., Herring, G., Madura, J.: General Chemistry: Principles and Modern Application, 9th edn., Printice Hall, New Jersey, Pearson2001.

Prospero, J. M., Landing, W. M., and Schulz, M.: African dust deposition to Florida: temporal and spatial variability and comparisons to models, J. Geophys. Res., 115, D13304, doi:10.1029/2009JD012773, 2010.

Reheis, M. C. and Kihl, R.: Dust deposition in southern Nevada and California, 1984–1989 – relations to climate, source area, and source lithology, J. Geophys. Res.-Atmos., 100, 8893–8918, 1995.

Reid, E. A., Reid, J. S., Meier, M. M., Dunlap, M. R., Cliff, S. S., Broumas, A., Perry, K., and Maring, H.: Characterization of African dust transported to Puerto Rico by individual particle and size segregated bulk analysis, J. Geophys. Res., 108, 8591, doi:10.1029/2002JD002935, 2003.

Ridame, C. and Guieu, C.: Saharan input of phosphate to the oligotrophic water of the open western Mediterranean Sea, Limnol. Oceanogr., 47, 856–869, 2002.

Scanza, R. A., Mahowald, N., Ghan, S., Zender, C. S., Kok, J. F., Liu, X., and Zhang, Y.: Modeling dust as component minerals in the Community Atmosphere Model: development of framework and impact on radiative forcing, Atmos. Chem. Phys. Discuss., 14, 17749–17816, doi:10.5194/acpd-14-17749-2014, 2014.

Schütz, L. and Rahn, K. A.: Trace element concentrations in erodible soils, Atmos. Environ., 16, 171–176, 1982.

Seinfeld, J. H. and Pandis, S. N.: Atmospheric Chemistry and Physics: from Air Pollution to Climate Change, J. Wiley, New York, 1998.

Shao, Y.: A model for mineral dust emission, J. Geophys. Res., 106, 20239–20254, doi:10.1029/2001jd900171, 2001.

Shen, Z. X., Li, X., Cao, J., Caquineau, S., Wang, Y., and Zhang, X.: Characteristics of clay minerals in Asian dust and their environmental significance, China Part., 3, 260–264, 2005.

BGD
11, 17491–17541, 2014

Shen, Z. X., Cao, J., Li, X., Okuda, T., Wang, Y., and Zhang, X.: Mass concentration and mineralogical characteristics of aerosolparticles collected at Dunhuang during ACE-Asia, Adv. Atmos. Sci., 23, 291–298, 2006.
Shen, Z. X., Cao, J. J., Arimoto, R., Zhang, R. J., Jie, D. M., Liu, S. X., Zhu, C.S.: Chemical composition and source characterization of spring aerosol over Horqin sand land in northeastern China, J. Geophys. Res., 112, D14315, doi:10.1029/2006JD007991, 2007.
Sillanpää, M.: Micronutrients and the Nutrient Status of Soils: a Global Study, FAO Soils Bulletin, No. 48., Appendix 6–7, Rome, 1982.
Stoorvogel, J. J., VanBreemen, N., and Janssen, B. H.: The nutrient input by Harmattan dust to a forest ecosystem in Côte d'Ivoire, Africa, Biogeochemistry, 37, 145–157, 1997.
Sun, Y., Zhuang, G., Yuan, H., Zhang, X., and Guo, J.: Characteristics and sources of 2002 super dust storm in Beijing, Chinese Sci. Bull., 49, 698–705, 2004a.
Sun, Y., Zhuang, G., Wang, Y., Han, L., Guo, J., Dan, M., Zhang, W., Wang, Z., and Hao, Z.: The air-borne particulate pollution in Beijing – concentration, composition, distribution and sources, Atmos. Environ., 38, 5991–6004, 2004b.
Svensson, A., Biscaye, P. E., and Grousset, F. E.: Characterizationof late glacial continental dust in the Greenland Ice Core Project ice core, J. Geophys. Res., 105, 4637–4656, doi:10.1029/1999jd901093, 2000.
Swap, R., Garstang, M., Greco, S., Talbot, R., and Kallberg, P.: Saharan dust in the Amazon Basin, Tellus B, 44, 133–149, 1992.
Textor, C., Schulz, M., Guibert, S., Kinne, S., Balkanski, Y., Bauer, S., Berntsen, T., Berglen, T., Boucher, O., Chin, M., Dentener, F., Diehl, T., Easter, R., Feichter, H., Fillmore, D., Ghan, S., Ginoux, P., Gong, S., Grini, A., Hendricks, J., Horowitz, L., Huang, P., Isaksen, I., Iversen, I., Kloster, S., Koch, D., Kirkevåg, A., Kristjansson, J. E., Krol, M., Lauer, A., Lamarque, J. F., Liu, X., Montanaro, V., Myhre, G., Penner, J., Pitari, G., Reddy, S., Seland, Ø., Stier, P., Takemura, T., and Tie, X.: Analysis and quantification of the diversities of aerosol life cycles within AeroCom, Atmos. Chem. Phys., 6, 1777–1813, doi:10.5194/acp-6-1777-2006, 2006.
Textor, C., Schulz, M., Guibert, S., Kinne, S., Balkanski, Y., Bauer, S., Berntsen, T., Berglen, T., Boucher, O., Chin, M., Dentener, F., Diehl, T., Feichter, J., Fillmore, D., Ginoux, P., Gong, S., Grini, A., Hendricks, J., Horowitz, L., Huang, P., Isaksen, I. S. A., Iversen, T., Kloster, S., Koch, D., Kirkevåg, A., Kristjansson, J. E., Krol, M., Lauer, A., Lamarque, J. F., Liu, X., Montanaro, V., Myhre, G., Penner, J. E., Pitari, G., Reddy, M. S., Seland, Ø., Stier, P., Takemura, T., and Tie, X.: The effect of harmonized emissions on aerosol properties in global models – an

BGD
11, 17491–17541, 2014

AeroCom experiment, Atmos. Chem. Phys., 7, 4489–4501, doi:10.5194/acp-7-4489-2007, 2007.
Titschack, J., Goetz-Neunhoeffer, F., and Neubauer, J.: Magnesium quantification in calcites [(Ca,Mg)CO_3] by Rietveld-based XRD analysis: revisiting a well-established method, Am. Mineral., 96, 1028–1038, 2011.
Wang, Q., Zhuang, G., Li, J., Huang, K., Zhang, R., Jiang, Y., Lin, Y., and Fu, J. S.: Mixing of dust with pollution on the transport path of Asian dust – revealed from the aerosol over Yulin, the north edge of Loess Plateau, Sci. Total Environ., 409, 573–581, 2010.
Werner, M., Tegen, I., Harrison, S. P., Kohfeld, K. E., Prentice, I. C., Balkanski, Y., Rodhe, H., and Roelandt., C.: Seasonal and interannual variability of the mineral dust cycle under present and glacial climate conditions, J. Geophys. Res., 107, D244744, doi:10.1029/2002JD002365, 2002.
Wilke, B. M., Duke, B. J., and Jimoh, W. L. O.: Mineralogy and chemistry of Harmattan dust in northern Nigeria, Catena, 11, 91–96, 1984.
Xuan, J., Sokolik, I. N., Hao, J., Guo, F., Mao, H., and Yang, G.: Identification and characterization of sources of atmospheric mineral dust in East Asia, Atmos. Environ., 38, 6239–6252, 2004.
Yadav, S. and Rajamani, V.: Geochemistry of aerosols of northwestern part of India adjoining the Thar Desert, Geochim. Cosmochim. Ac., 68, 1975–1988, 2004.
Zender, C., Bian, H., and Newman, D.: Mineral Dust Entrainment and Deposition (DEAD) model: description and 1990s dust climatology, J. Geophys. Res., 108, 4416, doi:10.1029/2002JD002775, 2003.
Zhang, X. Y., Arimoto, R., and An, Z. S.: Dust emission from Chinese desert sources linked to variation in atmospheric circulation, J. Geophys. Res., 102, 28041–28047, 1997.
Zhang, X. Y., Arimoto, R., Zhu, G. H., Chen, T., and Zhang, G. Y.: Concentration, size distribution and deposition of mineral aerosol over Chinese desert regions, Tellus B, 50, 317–330, 1998.
Zhang, X. Y., Gong, S. L., Shen, Z. X., Mei, F. M., Xi, X. X., Liu, L. C., Zhou, Z. J., Wang, D., Wang, Y. Q., and Cheng, Y.: Characterization of soil dust aerosol in China and its transport and distribution during 2001 ACE-Asia: 1. Network observations, J. Geophys. Res., 108, 4261, doi:10.1029/2002jd002632, 2003.

BGD
11, 17491–17541, 2014

Table 1a. Generalized mineral compositions (%) applied in this study.

Mineral	Mg	P	Ca	Mn	Fe	Al	Si	K
Smectite	1.21	0.17	0.91	0.03	2.55	8.57	27.44	0.27
Illite	0.85	0.09	1.45	0.03	4.01	10.47	24.11	4.28
Hematite	0.09	0.18	0.12	0.07	57.50	2.67	2.11	0.07
Feldspar	0.15	0.09	3.84	0.01	0.34	10.96	25.24	5.08
Kaolinite	0.02	0.16	0.03	0.01	0.24	20.42	20.27	0.00
Calcite	0.00	0.00	40.00	0.00	0.00	0.00	0.00	0.00
Quartz	0.00	0.00	0.00	0.00	0.00	0.00	46.70	0.00
Gypsum	0.00	0.00	23.30	0.00	0.00	0.00	0.00	0.00

BGD
11, 17491–17541, 2014

Table 1b. Elemental solubility as a percentage of the element contained in the minerals (%).

Mineral	Mg	P	Ca	Mn	Fe	Al	Si	K
Smectite	14.09	2.93	79.20	25.35	2.60	0.00	0.05	31.41
Illite	7.80	30.58	50.96	24.93	1.17	0.15	0.05	2.87
Hematite	0.00	0.00	0.00	3.39	0.01	0.00	0.00	0.00
Feldspar	5.17	0.00	4.46	4.71	3.01	0.12	0.02	4.53
Kaolinite	22.32	0.00	21.97	0.00	4.26	0.38	0.37	0.00
Calcite	0.00	0.00	7.00	0.00	0.00	0.00	0.00	0.00
Quartz	0.00	0.00	0.00	0.00	0.00	0.00	0.0003	0.00
Gypsum	0.00	0.00	0.56	0.00	0.00	0.00	0.00	0.00

Fe content came from Journet et al. (2008), the other elements were from personal communication with E. Journet, 2012.

BGD
11, 17491–17541, 2014

Table 2. Ten year averaged emission rates ($Tg\,yr^{-1}$) and percentages of elements over desert regions (%).

Source Regions	Mg ($Tg\,yr^{-1}$)	P ($Gg\,yr^{-1}$)	Ca ($Tg\,yr^{-1}$)	Mn ($Gg\,yr^{-1}$)	Fe ($Tg\,yr^{-1}$)	K ($Tg\,yr^{-1}$)	Al ($Tg\,yr^{-1}$)	Si ($Tg\,yr^{-1}$)	Dust ($Tg\,yr^{-1}$)
WAsia	0.91	177.27	12.73	35.28	5.53	3.70	16.71	72.43	251.17
NCAsia	0.50	92.73	6.05	18.03	2.26	1.90	8.36	37.99	128.59
CAsia	0.13	25.40	1.57	4.98	0.70	0.55	2.35	9.77	33.82
SCAsia	0.05	10.71	0.54	1.93	0.29	0.22	1.04	4.07	13.91
EAsia	0.21	43.78	1.62	8.16	1.28	0.85	4.22	18.27	58.90
Asian Region	**1.79**	**349.89**	**22.52**	**68.39**	**10.06**	**7.23**	**32.67**	**142.54**	**486.4**
ESah	1.23	273.68	11.98	48.28	6.62	5.41	26.45	102.59	346.16
WSah	2.62	531.45	30.67	100.75	14.25	11.04	50.35	208.70	712.00
SNAf	0.02	11.65	0.17	1.47	0.37	0.12	1.25	4.33	13.98
SAf	0.01	3.10	0.18	0.59	0.11	0.06	0.31	1.34	4.46
textbfAfrica	**3.89**	**819.88**	**42.99**	**151.09**	**21.34**	**16.63**	**78.36**	**316.96**	**1076.6**
NWNAm	0.00002	0.0047	0.0001	0.0008	0.0002	0.0001	0.0005	0.0019	0.030
SWNAm	0.02	3.01	0.16	0.60	0.10	0.07	0.29	1.27	4.20
North America	**0.02**	**3.02**	**0.16**	**0.60**	**0.10**	**0.07**	**0.29**	**1.27**	**4.2**
SAm	0.0005	0.12	0.01	0.02	0.003	0.002	0.01	0.04	0.15
Patag	0.03	6.79	0.27	1.32	0.20	0.13	0.62	2.82	9.08
South America	**0.03**	**6.91**	**0.27**	**1.34**	**0.21**	**0.13**	**0.63**	**2.86**	**9.2**
WAstr	0.0005	0.13	0.003	0.02	0.003	0.002	0.01	0.05	0.16
EAstr	0.02	5.13	0.20	0.91	0.16	0.10	0.48	1.78	6.11
Australia region	**0.02**	**5.26**	**0.20**	**0.93**	**0.17**	**0.10**	**0.49**	**1.83**	**6.3**
Global	**5.75**	**1184.96**	**66.14**	**222.34**	**31.87**	**24.15**	**112.44**	**465.46**	**1582.7**
Global mean % element	**0.36**	**0.07**	**4.18**	**0.01**	**2.01**	**1.53**	**7.10**	**29.41**	/
Min. % element in 15 SR*	0.17	0.07	1.19	0.01	1.67	0.86	6.50	28.84	/
Max. % element in 15 SR*	0.39	0.08	5.07	0.02	2.68	1.63	8.96	31.38	/

* SR refer to source regions.

BGD
11, 17491–17541, 2014

Table 3. Comparison of modeled and observed fractions of chemical elements in TSP and tuning ratio based on 13-sites measurements.

	Mg	P	Ca	Mn	Fe	K	Al
Corr. coeff. Of Averaged fractions	0.14	−0.32	0.75	−0.51	0.29	−0.16	0.72
Median of Obs. (%)	1.45	0.09	5.42	0.070	3.10	1.79	5.26
Median of Mod. (%)	0.43	0.08	3.41	0.020	2.29	1.54	7.81
Obs./Mod. Median Ratio	3.4	1.1	1.6	3.5	1.4	1.2	0.7

BGD
11, 17491–17541, 2014

Table 4. Fractions (%) of elements in dust deposition into ifferent ocean basins and ice sheets[a].

Ocean Basins/Glacier	Mg	P	Ca	Mn	Fe	K	Al	Si[b]
North Atlantic	1.43	0.10	5.36	0.06	3.05	1.89	5.96	28.32
South Atlantic	1.50	0.10	5.36	0.06	3.35	1.84	6.01	28.07
North Pacific	1.56	0.10	5.92	0.06	3.26	1.90	5.78	28.01
South Pacific	1.47	0.10	5.30	0.06	3.87	1.86	6.15	27.61
North Indian	1.38	0.08	7.90	0.05	3.13	1.81	4.95	28.29
South Indian	1.53	0.10	6.50	0.06	3.64	1.87	5.88	27.33
Southern Ocean	1.56	0.10	5.12	0.06	3.74	1.88	5.88	28.25
Arctic	1.60	0.10	6.23	0.06	3.31	1.96	5.76	27.76
Mediterranean	1.37	0.08	7.14	0.05	2.90	1.88	4.85	29.14
Antarctic ice sheets	1.50	0.10	4.90	0.06	3.54	1.82	5.55	29.17
Greenland ice sheets	1.50	0.09	7.49	0.06	2.82	1.89	5.24	28.00
Averaged	1.49	0.10	6.11	0.06	3.33	1.87	5.64	28.18

[a] After timing tuned ratios (Table 3) except for Si.
[b] Not tunned.

BGD
11, 17491–17541, 2014

Table 5. Comparison of modeled and observed fractions of chemical elements in TSP and tuning ratio based on 13-site measurements. Deposition of dust elements into different oceans and ice sheets*.

Ocean/ice sheet	Mg ($Tg\,yr^{-1}$)			P ($Gg\,yr^{-1}$)			Ca ($Tg\,yr^{-1}$)			Mn ($Gg\,yr^{-1}$)			Fe ($Tg\,yr^{-1}$)			K ($Tg\,yr^{-1}$)		
	Total	Sol-1	Sol-2	**Total**	Sol-1	Sol-2	**Total**	Sol-1	Sol-2	**Total**	Sol-1	Sol-2	**Total**	Sol-1	Sol-2	**Total**	Sol-1	Sol-2
North Atlantic	**1.50**	0.16	0.14	**103.12**	8.81	4.10	**5.64**	0.68	1.81	**58.90**	12.08	3.87	**3.20**	0.036	0.033	**1.99**	0.008	0.136
South Atlantic	**0.13**	0.01	0.02	**8.84**	0.79	0.38	**0.47**	0.06	0.17	**5.17**	1.07	0.34	**0.30**	0.003	0.003	**0.16**	0.007	0.014
North Pacific	**0.28**	0.03	0.03	**17.47**	1.66	0.65	**1.06**	0.13	0.33	**10.58**	2.25	0.58	**0.58**	0.007	0.006	**0.34**	0.014	0.025
South Pacific	**0.01**	0.001	0.001	**0.86**	0.07	0.04	**0.04**	0.006	0.01	**0.50**	0.10	0.03	**0.03**	0.0003	0.000	**0.02**	0.0007	0.001
North Indian	**0.56**	0.06	0.06	**34.38**	3.54	1.52	**3.23**	0.29	0.63	**21.86**	4.62	1.35	**1.28**	0.013	0.013	**0.74**	0.03	0.049
South Indian	**0.05**	0.005	0.005	**3.03**	0.30	0.20	**0.20**	0.02	0.05	**1.85**	0.39	0.16	**0.11**	0.001	0.001	**0.06**	0.002	0.004
Southern Ocean	**0.002**	0.0003	0.0003	**0.15**	0.01	0.01	**0.01**	0.001	0.003	**0.09**	0.02	0.01	**0.01**	0.0001	0.0001	**0.00**	0.0001	0.0002
Arctic	**0.02**	0.002	0.0020	**1.34**	0.13	0.05	**0.09**	0.01	0.02	**0.83**	0.18	0.04	**0.05**	0.0005	0.0004	**0.03**	0.001	0.002
Mediterranean	**0.18**	0.02	0.02	**10.66**	1.07	0.36	**0.92**	0.09	0.22	**6.76**	1.42	0.36	**0.37**	0.004	0.004	**0.24**	0.011	0.017
Antarctic ice sheets	**0.001**	0.0001	0.0001	**0.08**	0.007	0.003	**0.00**	0.001	0.002	**0.05**	0.01	0.003	**0.00**	0.00003	0.00003	**0.00**	0.0001	0.0001
Greenland ice sheets	**0.09**	0.01	0.01	**5.39**	0.49	0.21	**0.44**	0.04	0.10	**3.30**	0.71	0.19	**0.17**	0.002	0.002	**0.11**	0.005	0.007
Total	**2.83**	0.30	0.28	**185.32**	16.89	7.52	**12.11**	1.32	3.35	**109.89**	22.84	6.95	**6.10**	0.068	0.06	**3.69**	0.153	0.25

* After timing tuned ratio (Table 3).

BGD
11, 17491–17541, 2014

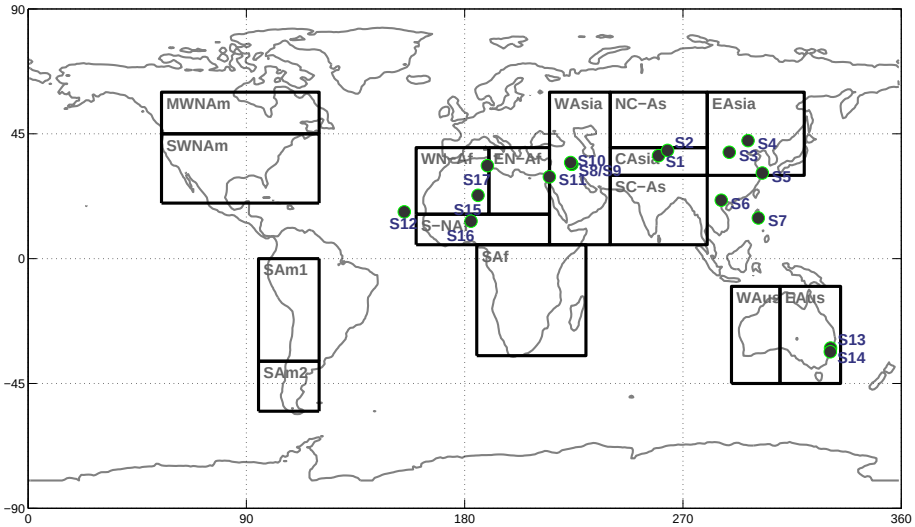

Figure 1. *Observational sites* (S1: Hetian, China; S2: Tazhong, China; S3: Yu Lin, China; S4: Duolun, China; S5: Shengsi, China; S6: Hanoi, Vietnam; S7: Marnila, Philippines; S8: Balad, Iraq; S9: Balad, Iraq; S10: Taji, Iraq; S11: Eilat; S12: Cape Verde Atmospheric Observatory (CVAO); S13: Muswellbrook, Australia; S14: Richmond, Australia; S15: Tamanrasset, Algeria; S16: Banizoumbou, Niger; S17-Douz, Tunisia) *and dust-producing regions* (WAsia: West Asia; NC-As: North Central Asia; CAsia:Central Asia; SC-As: South Central Asia; EAsia:East Asia; WN-Af: North West Africa; EN-Af: North East Africa; S-NAf: Southern North Africa; SAf: Southern Africa; MWNAm: Middle North West America; SWNAm: Southern North West America; SAm1: Northern South America; SAm2: Southern South America; WAus: West Austrilia; EAus: East Australia).

BGD
11, 17491–17541, 2014

Modeling the global emission, transport and deposition of mineral elements

Y. Zhang et al.

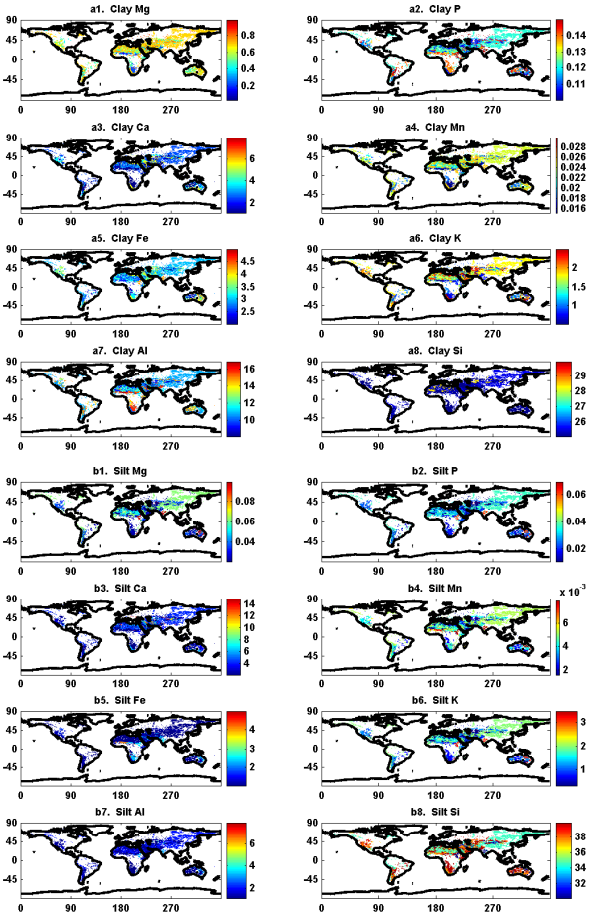

Figure 2. Global elemental distributions (in mass percentage) in a1: Clay Mg, a2: Clay P, a3: Clay Ca, a4: Clay Mn, a5: Clay Fe, a6: Clay K, a7:, Clay Al, a8: Clay Si; b1: Silt Mg, b2: Silt P, b3: Silt Ca, b4: Silt Mn, b5: Silt Fe, b6: Silt K, b7: Silt Al, b8: Silt Si.

BGD
11, 17491–17541, 2014

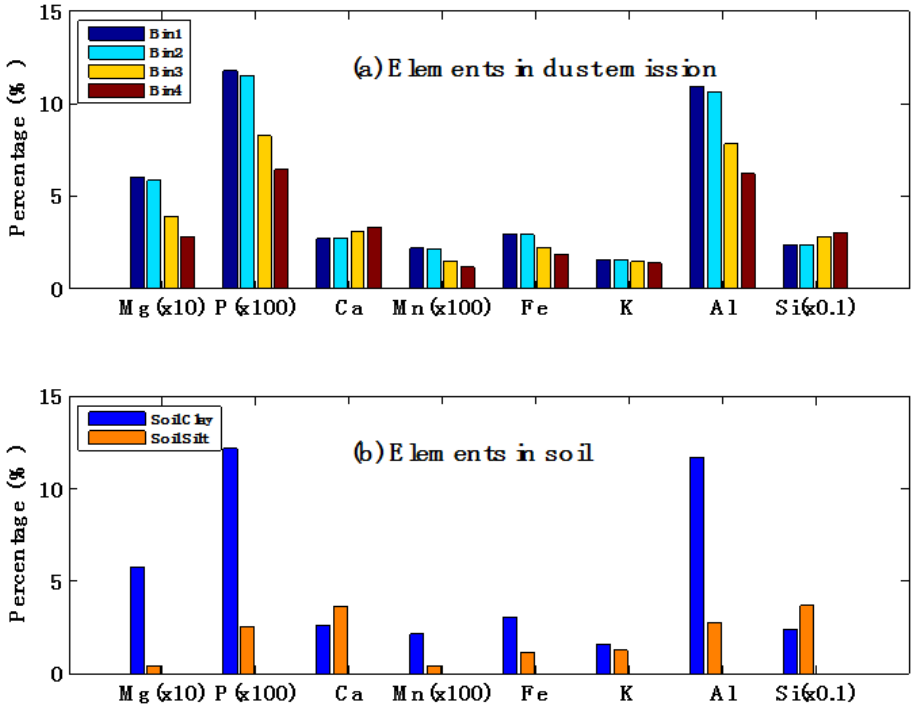

Figure 3. Global mean elemental percentages in **(a)** four-bin dust emission and **(b)** clay and silt fractions of soils (Bin1–4 refer to particle range listed in Table S2, clay refer to $< 2\,\mu m$, silt refer to $> 2\,\mu m$).

BGD
11, 17491–17541, 2014

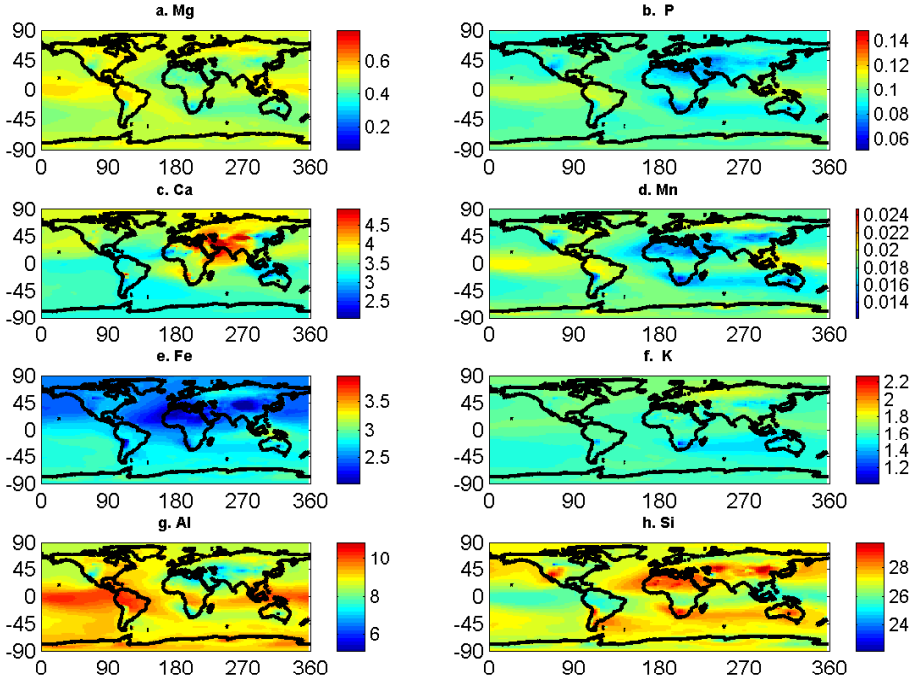

Figure 4. Percentages of elements in dust concentration mass %: **(a)** Mg, **(b)** P, **(c)** Ca, **(d)** Mn, **(e)** Fe, **(f)** K, **(g)** Al, **(h)** Si.

BGD
11, 17491–17541, 2014

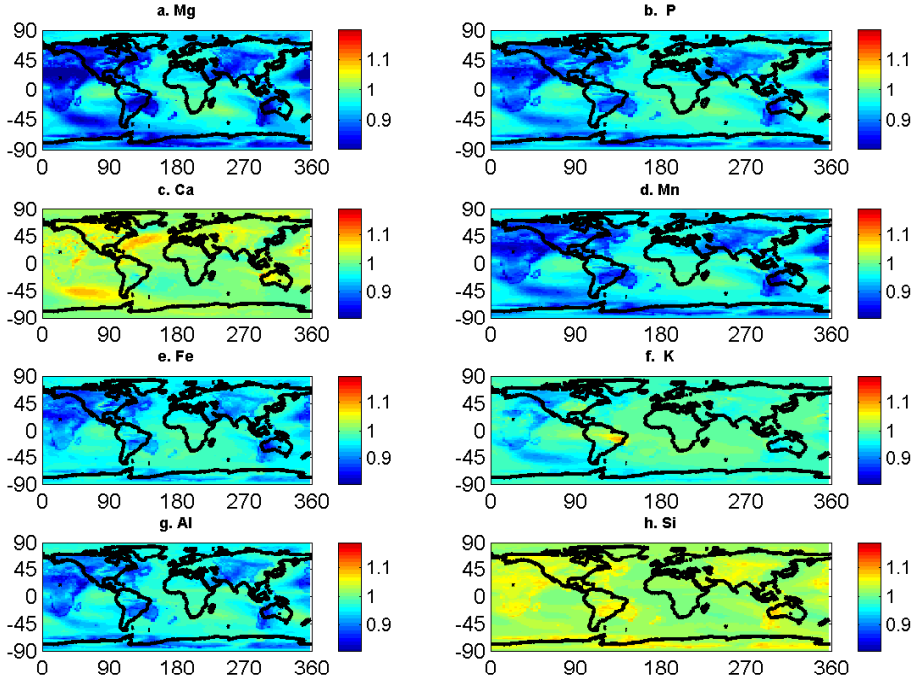

Figure 5. Ratio of mass fractions of elements in dust deposition to that in atmospheric dust: **(a)** Mg, **(b)** P, **(c)** Ca, **(d)** Mn, **(e)** Fe, **(f)** K, **(g)** Al, **(h)** Si.

BGD
11, 17491–17541, 2014

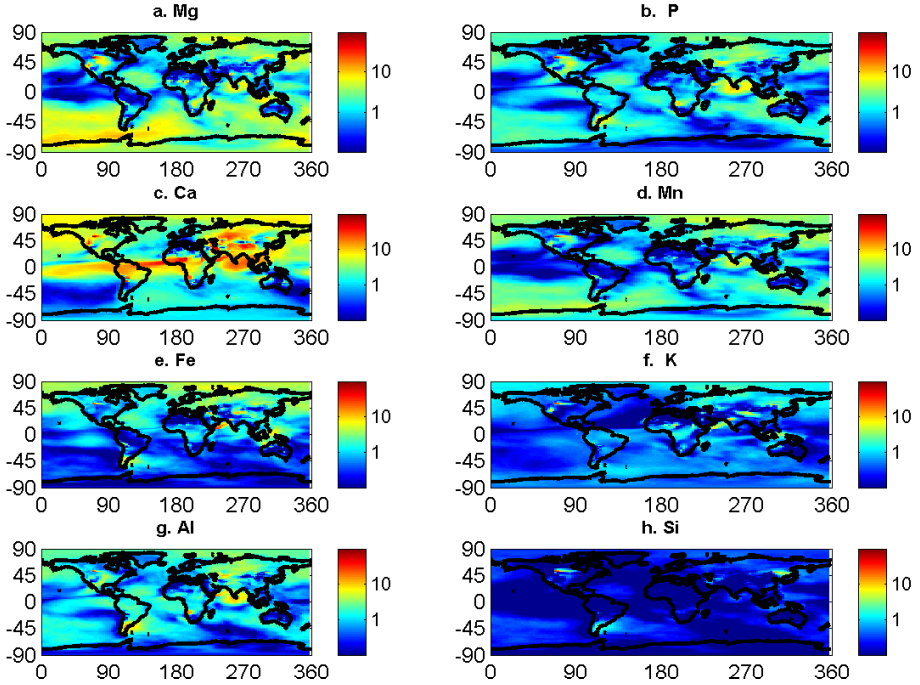

Figure 6. Ten-year monthly variability in mean of elemental percentages in atmospheric dust (mass %): **(a)** Mg, **(b)** P, **(c)** Ca, **(d)** Mn, **(e)** Fe, **(f)** K, **(g)** Al, **(h)** Si.

BGD
11, 17491–17541, 2014

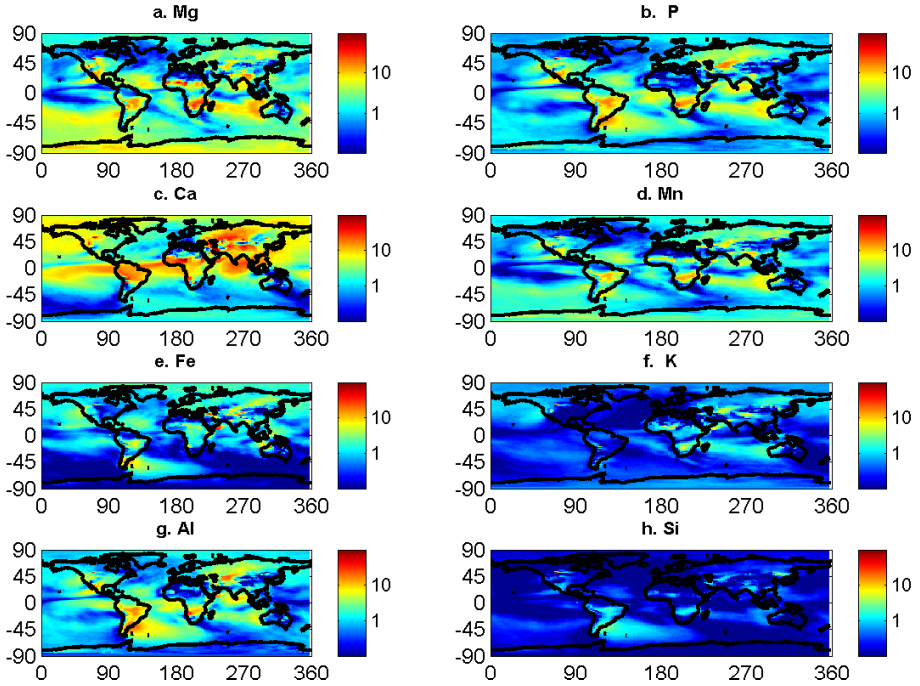

Figure 7. Ten-year monthly variability in mean of elemental percentages in dust depostion (mass %): **(a)** Mg, **(b)** P, **(c)** Ca, **(d)** Mn, **(e)** Fe, **(f)** K, **(g)** Al, **(h)** Si.

BGD
11, 17491–17541, 2014

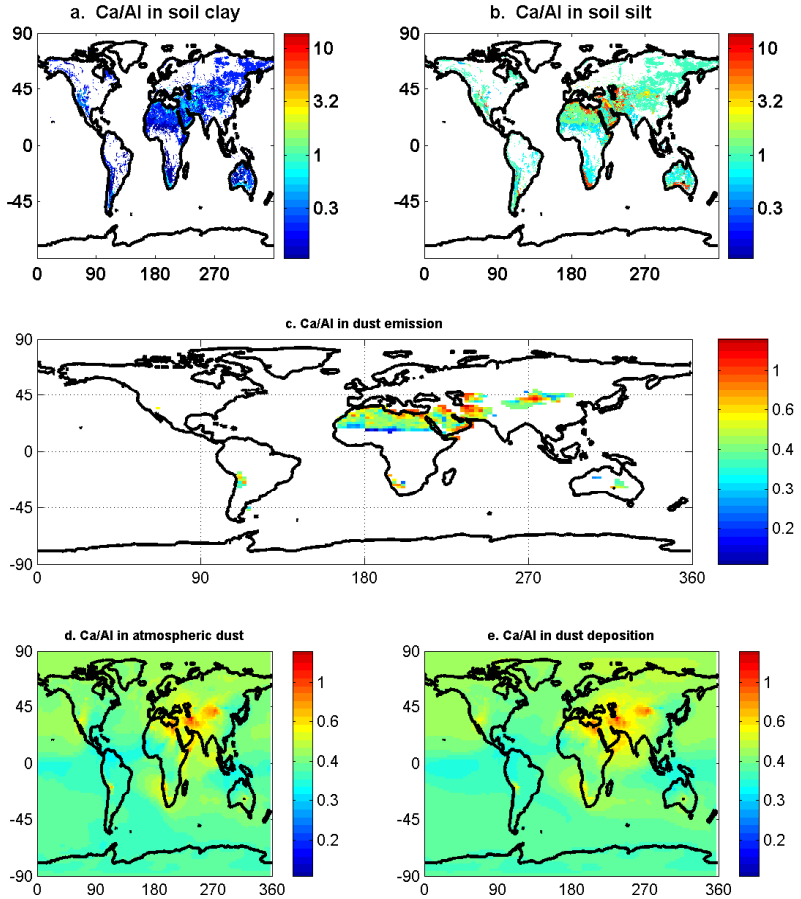

Figure 8. Ca/Al in soil and ten year averaged Ca/Al ratio in dust emission, concentration and deposition. Top two **(a, b)** refer to ratio in clay and silt desert soil, middle one **(c)** refer to ratio in dust emission, and bottom two **(d, e)** refer to ratio in dust concentration and deposition.

BGD
11, 17491–17541, 2014

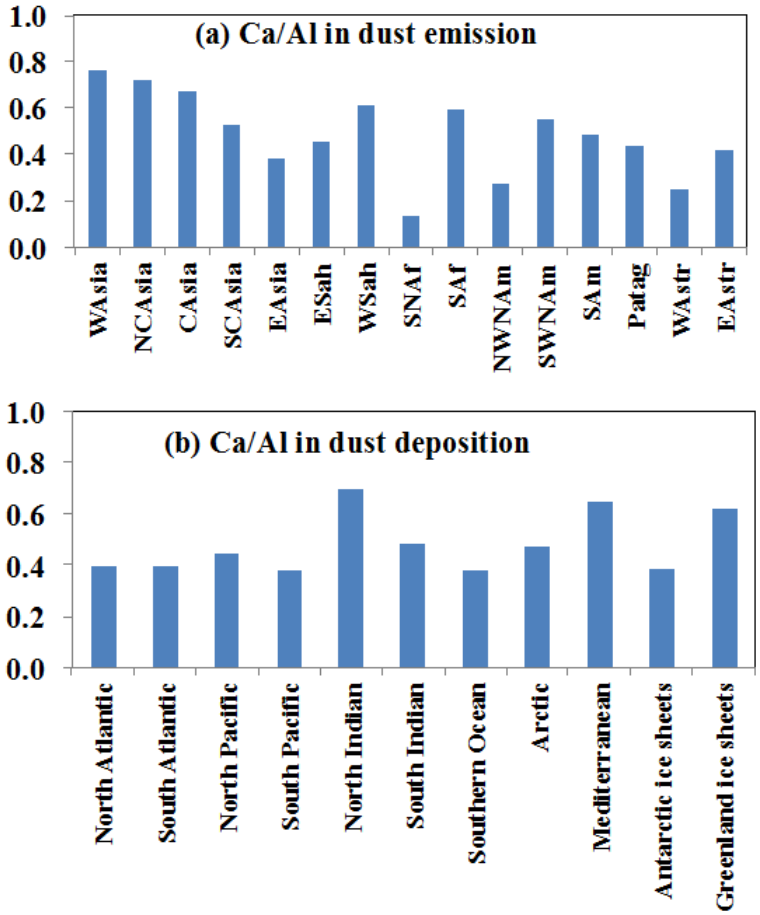

Figure 9. Ten year averaged Ca/Al ratio in **(a)** dust emission of source regions and **(b)** dust deposition into various ocean basins and glaciers.

BGD
11, 17491–17541, 2014

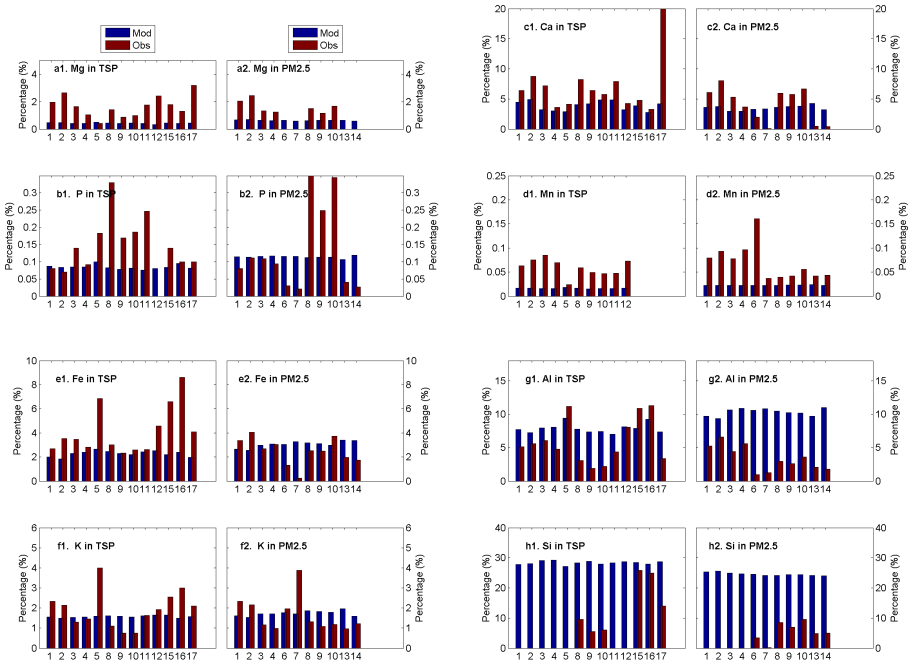

Figure 10. Comparison of observed and modeled mean fractions of elements at each site for total suspended particulates (TSP). (1 – Hetian, China; 2 – Tazhong, China; 3 – Yu Lin, China; 4 – Duolun, China; 5 – Shengsi, China; 6 – Hanoi, Vietnam; 7 – Marnila, Philippines; 8 – Balad, Iraq; 9 – Baghdad, Iraq; 10 – Taji, Iraq; 11 – Eilat; 12 – Cape Verde Island; 13 – Muswellbrook, Australia; 14 – Richmond, Australia, 15 – Tamanrasset, Algeria; 16 – Banizoumbou, Niger; 17 – Douz, Tunisia).

BGD
11, 17491–17541, 2014

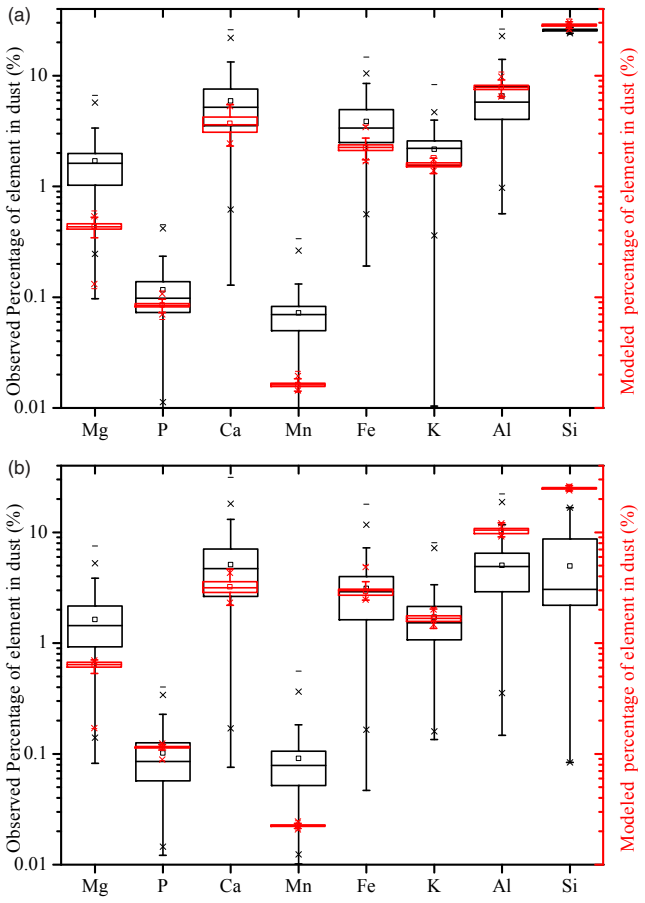

Figure 11. Mean and quartile modeled and observational fractions of elements in **(a)** TSP and **(b)** $PM_{2.5}$ for all sites together, the box line presents 25, 50 and 75 %, individually.

BGD
11, 17491–17541, 2014

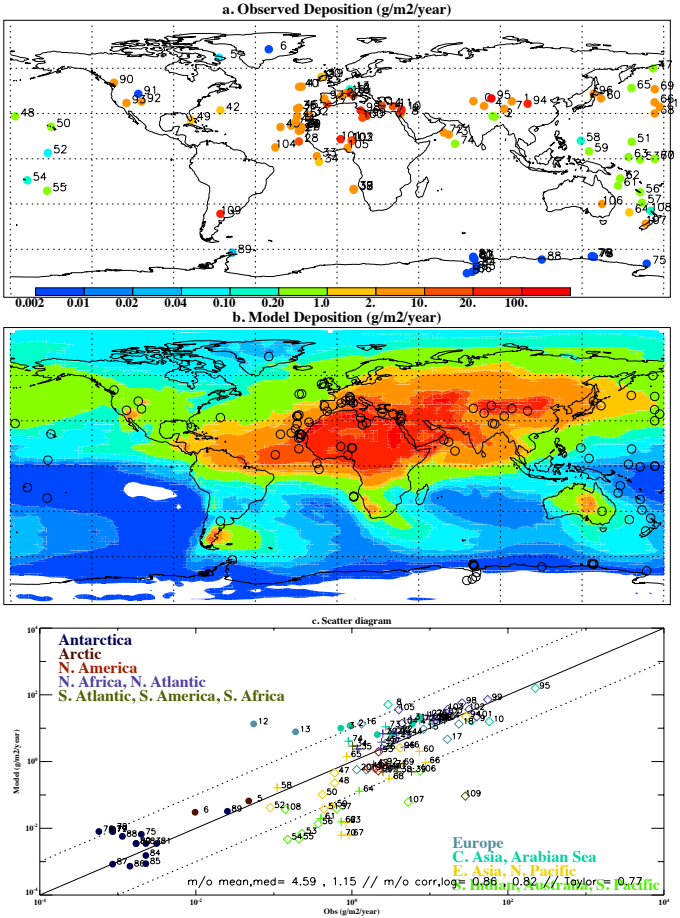

Figure 12. (a) Observational and **(b)** modeled dust deposition ($g\,m^{-3}\,yr^{-1}$). The scale is the same for both panels. **(c)** A scatter plot shows the comparison between the model and observations. The correlation coefficient between observations and model results reach 0.86.

BGD
11, 17491–17541, 2014

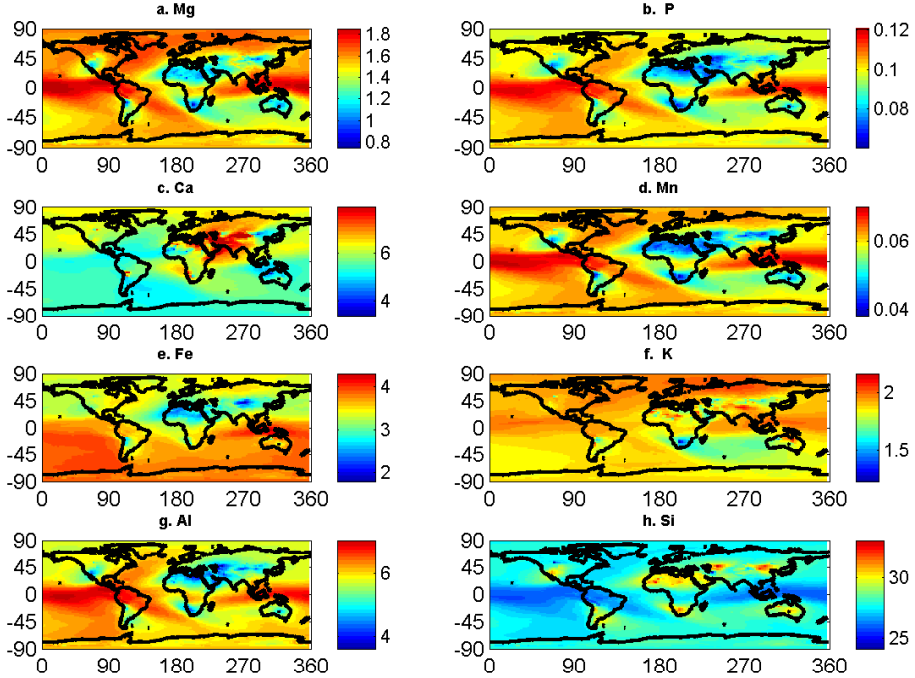

Figure 13. Tuned percentages of elements in dust deposition (%). It is tuned based on original percentages of elements in dust deposition in Fig. S1 by ratioing Obs./Mod. ratios listed in Table 3. Si did not change because there are not enough observational data available.

BGD
11, 17491–17541, 2014

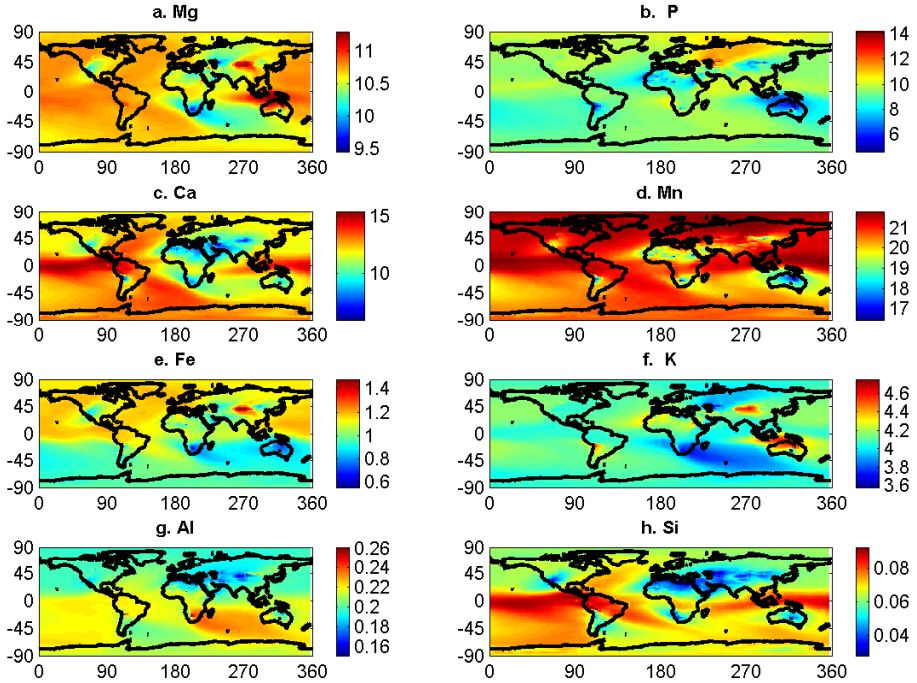

Figure 14. Fractional solubility of elements (soluble element/total element) in dust deposition (%): **(a)** Mg, **(b)** P, **(c)** Ca, **(d)** Mn, **(e)** Fe, **(f)** K, **(g)** Al, **(h)** Si.

BGD
11, 17491–17541, 2014

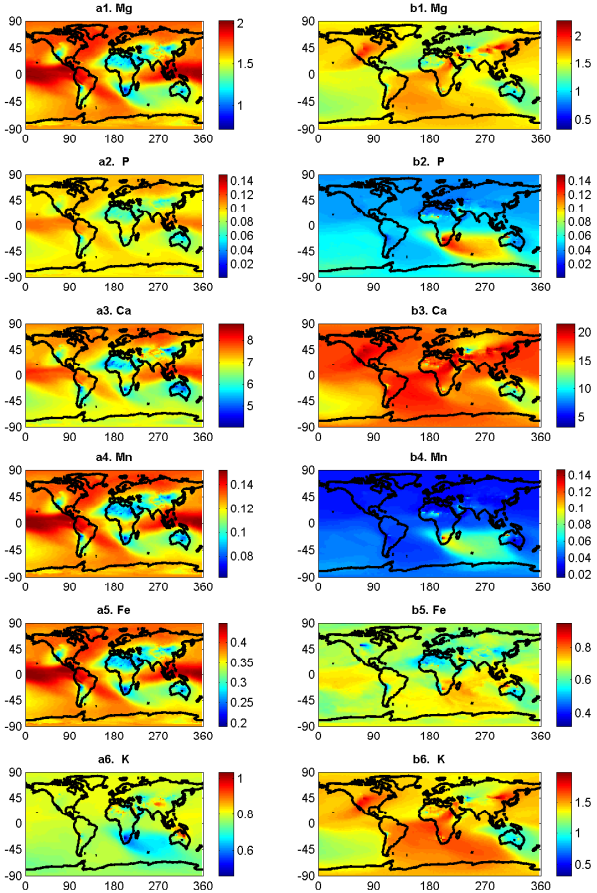

Figure 15. Proportions (‰) of soluble elements in total dust deposition using **(a)** M1 and **(b)** M2, M1 refer to mineral method after tuning, M2 refer to Sillanpää method described in the Sect. 2.

BGD
11, 17491–17541, 2014